Evaluating Polymers Interplay to Investigate Lignocellulose Recalcitrance

Amandine Leroy
INRAE UR BIA 44316 Nantes; Université de Reims CHampagne-Ardenne, INRAE, FARE, UMR A614 51097 Reims

Xavier Falourd
INRAE UR BIA 44316 Nantes

Loïc Foucat
INRAE UR BIA 44316 Nantes

Valérie Méchin
INRAE Institut Jean-Pierre-Bourgin 78026 Versailles

Fabienne Guillon (fabienne.guillon@inrae.fr)
INRAE UR BIA 44316 Nantes https://orcid.org/0000-0001-7925-3104

Gabriel Paës
Universite de Reims Champagne-Ardenne, INRAE, FARE, UMR A614

Research Article

Keywords: Biomass recalcitrance, molecular and structural factors, hot water pretreatment (HWP), maize stem, NMR analysis

Posted Date: May 6th, 2021

DOI: https://doi.org/10.21203/rs.3.rs-452185/v1

Version of Record: A version of this preprint was published at Biotechnology for Biofuels on July 31st, 2021. See the published version at https://doi.org/10.1186/s13068-021-02015-8.

Evaluating polymers interplay to investigate lignocellulose recalcitrance

Amandine Leroy[1,4], Xavier Falourd[1,2], Loïc Foucat[1,2], Valérie Méchin[3], Fabienne Guillon[1]*, Gabriel Paës[4]*

[1]*INRAE, UR 1268 BIA, 44316 Nantes, France*

[2]*INRAE, BIBS Facility, 44316, Nantes, France*

[3]*INRAE, Institut Jean-Pierre Bourgin, 78026 Versailles, France*

[4]*Université de Reims Champagne Ardenne, INRAE, FARE, UMR A614, 51097 Reims, France*

* Corresponding authors

Introduction:

Valorisation of lignocellulosic biomass (LB) is a promising way to develop a sustainable bioeconomy and thus to reduce our carbon footprint on the environment **(1)**. Each year, more than 1.3 trillion tons of LB is generated worldwide and only 3% of this resource is valorised **(1, 2)**. The high energy content is the main interest of LB, allowing it to be on the long-term economically competitive with fossil resources **(3)**. In fact, more than 90% of LB is composed of three highly connected polymers: cellulose, hemicelluloses and lignin. In the biorefinery concept, pretreatment, enzymatic hydrolysis and fermentation steps can convert these polymers into various bioproducts such as high added value molecules, materials or energy **(3-5)**. In spite of this high potential, valorisation of LB is still limited by its recalcitrance against hydrolytic

deconstruction by enzymes, hampering the release of fermentable sugars, precursors of biosourced products **(6, 7)**.

Biomass accessibility is considered as the main factor of recalcitrance and is influenced by various factors specific to the LB which are difficult to apprehend due to their strong interconnections **(7-9)**. Within these factors contributing to recalcitrance, a distinction can be made between factors related to the composition of the LB, such as the content of hemicelluloses or lignin, and structural factors, including porosity, specific surface area of the cellulose as well as ultrastructural factors related to cellulose (crystallinity, the degree of polymerisation) **(7)**. Pretreatment goal is precisely to reduce LB recalcitrance by "opening" the polymer network thus improving the accessibility of the enzymes to the LB, and more notably to cellulose **(4, 10)**. Over the last decades, various pretreatments have been developed to break down and restructure the lignocellulosic matrix **(8, 11, 12)**. These pretreatments can be organized into four categories: physical (milling, ultra sound, etc), chemicals (ionic liquid, dilute acid, organosolv, etc), physico-chemical (steam explosion, hot water, oxidative, etc) and biological (fungi, bacteria or archaea) pretreatments **(11, 13, 14)**. Among the physico-chemical pretreatments, hot water pretreatment (HWP), also called hydrothermal pretreatment or autohydrolysis, stands out from the crowd **(15-17)**. HWP uses as sole catalyst hot water, generally between 170–230 °C, which is kept in liquid state by the application of a high pressure of up to 5 MPa for the highest temperatures **(13, 18)**. The absence of corrosive compounds allows HWP to be one of the most economical, easy to implement and environmentally friendly pretreatments **(18)**.

Several studies have investigated the effect of HWP in order to obtain a better understanding of the factors contributing to LB recalcitrance. Most commonly, the effect of HWP is analysed

on the basis of the variation of the chemical composition of the LB. It is now well known that hemicelluloses is the main polysaccharide fraction impacted by the HWP **(17)**. Indeed due to their amorphous structure, hemicelluloses are the most susceptible components to be hydrolysed through the breaking of glycosidic bonds by organic acids generated during the pretreatment **(3, 18)**. HWP also induces changes within other lignocellulosic components, including lignin and hydroxycinnamic acids, through the breakdown of inter- and intra-polymer bonds involving ferulic acid molecules **(18-20)**. These chemical modifications have been shown to induce an increase in the deconstruction capacity of the enzymes through their direct impact on the structural parameters of the lignocellulosic matrix. As a matter of fact, three length-scales of structural modifications can be considered: the cell wall porosity (associated to the mobility of enzymes), the polymers' interactions and the polymers' ultrastructure **(21-23)**. Several methods have been proposed to study the porosity of the LB, using different probes such as polymers in solute exclusion technique **(24)**, water molecules in NMR relaxometry (low-field NMR) or mercury in porosimetry **(25-27).** Other techniques are used to have an indirect estimation of porosity such as Simons' staining, using dyes with a high affinity for cellulose, and also allowing to estimate the accessible surface area of cellulose for cellulase adsorption during enzymatic hydrolysis **(28)**. Information on cellulose ultrastructure and interplays with the other components of LB can be obtained thanks to solid-state-NMR. However, relatively few studies have exploited the potential of this method to analyse changes in polymer composition and organization within the cell wall following the application of HWP **(29)**, whereas they have contributed to new progresses for other polymer interactions **(30)**. Overall, despite their importance, the interplay between chemicals and structural factors that control HWP and contribute to recalcitrance is still not understood.

In this study, the impact of HWP on the different factors that are associated with LB recalcitrance was examined by implementing complementary methods that probe different levels of structure. Simons' staining, solid-state NMR and low-field NMR analyses were combined to assess porosity, water-biomass interaction and to characterise the structure and the environment of the cellulose. Due to their agricultural and economic importance, maize residues were chosen as a model of grass LB.

Results and discussion:

1/ Influence of HWP on saccharification profiles

Fig. 1: Kinetics of released monosaccharides yield during saccharification of raw and HWP samples.

For both genotypes, HWP induced an increase in the conversion of sugars, and this improvement was higher as the pretreatment time increased **(Fig. 1)**. The percentage of sugars converted during the saccharification was increased by 1.7 to 4.6 fold compared to the raw material according to genotype and HWP time, which is in agreement with results reported in the literature on corn straw **(31)** or other grasses species such as sugarcane **(15, 32),** wheat and miscanthus **(26)**. The initial reaction rates were also increased by 1.2 and 2.4 fold for M7 and by 2.2 and 3.6 fold for M9 with the increase of the pretreatment time from 20 to 40 min. These observations show that HWP increases the accessibility and hydrolysis capacity of the hydrolytic enzymes, as described below.

2/ Modifications of the chemical composition and of the structure of cell wall polymers

A- Modifications of the chemical composition

97 The compositional changes occurring upon HWP were first determined by FTIR spectra
98 combined with chemical analyses.

99 **Fig.2:** FTIR spectra of raw and pretreated (a) M7 and (b) M9 samples.

100 The two genotypes had differing absorbance profiles in the spectral region from 800 cm^{-1} to
101 1200 cm^{-1}, corresponding to the region of polysaccharide absorption **(33)** and at 1515 cm^{-1},
102 characteristic of C=C stretching of lignins **(Fig. 2)**. Indeed, the absorbance in the sugar region
103 was more important in genotype M7, highlighting a higher sugars content within this genotype.
104 In contrast, the peaks characteristic of lignin was higher in genotype M9, showing an
105 enrichment of lignin in this genotype.

106 Following HWP, a decrease in the absorption between 800-1200 cm^{-1} was observed **(Figure**
107 **2)**. Indeed, the absorbance at 1053 cm^{-1}, which is typical of the C-O stretching band of linear
108 or branched β-(1,4) xylans, decreased with an increase of HWP time. This likely corresponds
109 to a decrease of the glucuronoarabinoxylans (GAX) content in the CWR **(34-36)**. The decrease
110 in GAX content induced an enrichment in cellulose and lignin, as shown by the appearance of
111 the peak at 1032 cm^{-1}, corresponding to the C-O stretching signal of β-(1-4) glucans, and the
112 increase of the peak at 1515 cm^{-1}. The variation of non-conjugated esters from polysaccharide
113 components was shown at the wavelengths of 1735 cm^{-1} and 1250 cm^{-1} **(37)**. Interestingly, the
114 absorbance of these bands was increased with HWP 20 min, then decreased with HWP 40 min
115 for both genotypes.

116

117

118

Table 1: Composition of CWR and percentage of solubilized or lost macromolecular fractions after the HWP.

	Raw maize stem		HWP 20 min		HWP 40 min	
	M7	M9	M7	M9	M7	M9
Pretreatment severity	-	-	3.66	3.66	3.96	3.96
Yield of HWP ($g.g^{-1}$ CWR)	-	-	0.797 (± 0.022)	0.796 (± 0.034)	0.629 (± 0.027)	0.636 (± 0.033)
Hydrolysate pH	-	-	4.4 (± 0.06)	4.4 (± 0.08)	3.8 (± 0.01)	3.8 (± 0.06)
Composition						
Polysaccharides ($g.100g^{-1}$ CWR)	60.2 (± 0.7)	67.3 (± 1.5)	65.7 (± 1.9)	62,1 (± 4.4)	65.1 (± 2.6)	64.0 (± 0.3)
Cellulose ($g.100g^{-1}$ of sugars)	67.7 (± 0.1)	62.1 (± 0.4)	58.4 (± 0.1)	62.4 (± 0.3)	76.7 (± 0.3)	69.2 (± 0.8)
Hemicelluloses ($g.100g^{-1}$ of sugars)	32.3 (± 0.1)	37.9 (± 0.4)	41.6 (± 0.1)	37.6 (± 0.3)	23.3 (± 0.3)	30.8 (± 0.8)
Klason lignin ($g.100g^{-1}$ CWR)	16.3 (± 0.1)	18.6 (± 0.4)	18.7 (± 0.2)	20.1 (± 0.3)	25.3 (± 1.3)	27,3 (± 0.2)
Loss/solubilization after HWP[a]						
Cellulose (%)	-	-	25.3 (± 1.5)	23.9 (± 5.3)	23.1 (± 1.0)	30.6 (± 0.8)
Hemicelluloses (%)	-	-	13.4 (± 3.2)	19.6 (± 4.2)	50.5 (± 3.4)	45.7 (± 1.1)
Klason lignin (%)	-	-	8.7 (± 1.0)	11.8 (± 1.1)	3 (± 0.4)	6.6 (± 0.7)

Results are expressed as means of three repetitions with standard deviation into parentheses.

[a] Loss/solubilization after HWP (%) = $100\times[1-MY\times(Y_f/Y_i)]$, where MY is the mass yield of the HWP, Y_f is the final content and Y_i is the initial content (raw CWR).

For raw M7 and M9 CWR, polysaccharide content, lignin content and the cellulose/hemicelluloses ratio were 60.2/67.3%, 16.3/18.6% and 2.09/1.64, respectively (Table 1). For hemicelluloses, ^{13}C CP/MAS NMR analyses showed that the molar proportion of hemicelluloses, expressed relative to the sum of hemicelluloses and cellulose, remains stable after a HWP 20 min and then decreases by 6% and 4% after the 40 min HWP **(Table 2)**. The non-reduction of the molar proportion of hemicellulose after 20 min pretreatment may be related to an equivalent molar loss of cellulose for this severity of pretreatment. Through the quantification of sugars by HPAEC-PAD **(Table 1)**, a decrease in the relative hemicellulose content according to the time of the HWP, was detected. This decrease corresponded to a GAX solubilization of 13.4% and 50.5% for the M7 and of 19.6% and 45.7% for the M9 genotype compared to the GAX content in the raw materials for the HWP 20 min and HWP 40 min, respectively. The removal of the hemicelluloses fraction during HWP was achieved by the hydrolysis of glycosidic bonds within the xylan backbone via hydronium ions and organic acids produced by the auto-ionization of water and the release of organic acids (acetic acid) and uronic acids **(18, 38)**.

In contrast, HWP induced a cellulose enrichment of up to 11.7% and 10.3% in HWP 40 min for genotypes M7 and M9, respectively. A solubilization between 23.1-30.6% of the cellulose was detected with the application of the HWP. This loss was slightly higher than those found in another study on corn stover **(31)** (between 4-22% **(18, 39)**).

Besides, the lignin relative content increased by 7.5-13% with HWP 20 min and 31.8-35.5% with HWP 40 min according to the genotype. A minor loss of lignin was observed for HWP CWR ranging from 3 to 11.8%. Lignin solubilization was more pronounced for the 20 min HWP, and may suggest a depolymerization/repolymerization of lignin according to the HWP

147 time due to the acidification of the medium leading to the breaking of carbohydrate-lignin
148 bonds (**38, 40, 41**).

149 These analyzes showed that the HWP induced changes in the relative content of the three main
150 polymers, with a loss of hemicelluloses. This could impact the composition and/or structure of
151 the lignin–carbohydrate complex (LCC) and indirectly the hydrolysis capacity (**41**).

152 **Table 2:** CP/MAS ^{13}C NMR analysis of molar proportion of hemicellulose.

	Raw maize stem		HWP 20 min		HWP 40 min	
	M7	M9	M7	M9	M7	M9
Hemicelluloses molar proportion (%)	21 (± 2)	20 (± 1)	20 (± 1)	19 (± 1)	15 (± 0)	16 (± 2)

153 Results are expressed as means of three repetitions with standard deviation into parenthesis.

154 B- Impact on the phenolic compounds

155 **Table 3:** Ester- and ether-linked hydroxycinnamic acid content in raw and HWP CWR.

	Raw maize stem		HWP 20 min		HWP 40 min	
	M7	M9	M7	M9	M7	M9
p-coumaric acid (g.100g^{-1} CWR)						
Ester linked	2.58 (± 0.4)	2.20 (± 0.6)	2.87 (± 0.2)	2.66 (± 0.7)	2.76 (± 0.2)	2.31 (± 0.1)
Ferulic acid (g.100g^{-1} CWR)						
Ester linked	0.55 (± 0.01)	0.50 (± 0.01)	0.71 (± 0.01)	0.60 (± 0.02)	0.42 (± 0.01)	0.34 (± 0.01)
Diferulic acid ester linked	0.11 (± 0.01)	0.09 (± 0.01)	0.15 (± 0.01)	0.09 (± 0.01)	0.02 (± 0.01)	0.02 (± 0.01)
Ether linked	0.44	0.42	0.27	0.34	0.37	0.39

156 Results are expressed as means of three repetitions with standard deviation into parenthesis.

157 Grasses are rich in hydroxycinnamic acid ester- and ether-bounded, mainly ferulic acid (FA)
158 and *p*-coumaric acid (*p*-CA) **(42, 43)**. The content of FA and *p*-CA ether- and ester-bounded
159 was determined (**Table 3**).

160 *p*-CA is mainly linked to the side chain of the lignin syringyl units and, to a lesser extent, to
161 the GAX arabinose units **(44)**. The *p*-CA content in the raw and HWP CWR remained stable,
162 representing between 2.2-2.8% of their CWR. The *p*-CA stability, despite an enrichment in
163 lignin, suggests that HWP induced a homogeneous *p*-CA solubilization according to the mass
164 loss between 4-11% for the 20 min HWP and 33% for the 40 min HWP.

165 Within the cell wall, phenolic compounds are closely bound to carbohydrates through
166 numerous bonds forming LCCs. In grasses, ferulic acid is the cross-linking agent that mainly
167 allows the formation of these complexes by forming GAX-GAX bonds via esterified diferulic
168 acids (DiFAe) on arabinose units and GAX-lignin bonds via ether bonds on guaiacyl units of
169 lignin **(44-46)**. Numerous studies have shown that this complex network formed by the cross-
170 linking of FAs between hemicelluloses and lignin leads to a decrease of the polysaccharides
171 deconstruction by limiting the access to the enzymes **(47)**.

172 In the raw genotypes, about 60% of FA units were found to be linked to arabinose while 40%
173 were engaged in ether linkages with lignin. The DiFAe content, related to the number of
174 hemicellulose bonds, decreased significantly by more than 88% after the HWP 40 min.
175 Interestingly, with the HWP 20 min, the amount of DiFAe binding remained stable in the M7
176 CWR and decreased slightly by 19% on M9 CWR. This difference between the two genotypes
177 shows that the HWP 20 min allows a more efficient disruption of the hemicellulosic network
178 in M9, which is consistent with the higher hemicelluloses loss in this genotype.

179 The content of GAX-lignin bonds could be estimated via the content of FA ether linked.
180 Contrary to the GAX-GAX bonds, a significant amount of AX-lignin bonds was broken after

20 min of the HWP. As observed for lignins, the loss of etherified FA was more important after HWP 20 min with 50/36% than after HWP 40 min with 46/40% for M7 and M9 respectively. This likely originates from a depolymerization/re-polymerization or reorganisation of the lignins during the pretreatment. In addition, these results suggest that HWP induces sequential changes on the LCC with a prior step of GAX-lignin disruption followed by the GAX-GAX perturbations, as already suggested **(48)**. This hypothesis is strengthened by the low loss of hemicelluloses and the higher loss of lignin at a HWP time of 20 min, highlighting a prior disruption of the lignin fraction. However, it should be noted that the amount of FA engaged in ether bonds with lignin could be underestimated due to the lignin complexity which may prevent the hydrolysis of total FA ether linked.

C- Modification of the polymers ultrastructure

In order to determine the influence of the parameters specific to the composition of the lignocellulose on the structural modifications, a correlation matrix was carried out and is presented in **Additional file 1**.

1- Lignin

202 **Table 4:** Lignin characteristics: thioacidolysis yield, S/G ratio and fluorescence intensity.

203

	Raw maize stem		HWP 20 min		HWP 40 min	
	M7	M9	M7	M9	M7	M9
Thioacidolysis yield ($\mu mol.g^{-1}$ KL)	765 (± 23)	671 (± 43)	799 (± 11)	884 (± 12)	321 (± 33)	266 (± 8)
S/G ratio	1.79 (± 0.02)	1.02 (± 0.03)	1.96 (± 0.14)	0.99 (± 0.01)	2.87 (± 0.10)	1.35 (± 0.10)
Fluorescence intensity	8100	5500	4700	2600	1700	1200

204 Thioacidolysis yields are expressed in $\mu mol.g^{-1}$.Klason Lignin. Syringyl/Guaiacyl molar ratio (S/G ratio) are determined by
205 thioacidolysis. Fluorescence intensity was measured at $\lambda_{excitation}$= 365 nm and $\lambda_{emission}$= 440 nm. Results are expressed as means
206 of three repetitions with standard deviation into parenthesis.

207 As shown by the hydroxycinnamic acids and lignin loss, the HWP could have an impact on the
208 organisation of the lignin depending on the severity of the pretreatment. The fluorescence
209 intensity of the CWR, relative to the overall structural properties of the lignin, was carried out
210 **(Table 4)**. A decrease of the fluorescence intensity of about 42-53% and 79% was detected for
211 HWP 20 min and HWP 40 min, respectively, in comparison to raw CWR. Given that the
212 intensity of fluorescence of the CWR depends on the composition of the lignin, type and
213 content of the bonds between the monolignols and lignin environment **(49)**, this result suggests
214 HWP leads to a global structural/compositional modification of the lignin fraction.

215 The ultrastructural modification of the lignin was analysed in more details through the analysis
216 of the thioacidolysis yield and the syringyl/guaiacyl lignin units (S/G) ratio (**Tables 4)**. For raw
217 M7 and M9, thioacidolysis yield and S/G ratio were 764/672 $\mu mol.g^{-1}$ of Klason lignin and

1.79/1.02 respectively: this means that M7 had a higher β-O-4 bonds and S units content. Even if the loss of lignin induced by HWP was limited (less than 12%), changes in the lignin structure have occurred. Indeed, the yield of thioacidolysis, based only on the cleavage of non-condensed ether β-O-4 bonds which are predominant in grasses **(50)**, was decreased significantly by 58% and 60% with the HWP 40 min for M7 and M9, respectively. The S/G ratio was gradually impacted by HWP with an increase according to severity. The content of G units falls down with the 40 min pretreatment. This suggests that the β-O-4 links of the G units, determined by thioacidolysis, were more impacted by HWP and therefore more susceptible to the condensation than the S units, as already shown on rice and sugarcane bagasse **(51, 52)**.

Table 5: CP/MAS and VCT ^{13}C NMR analysis of raw and pretreated CWR.

	Raw maize stem		HWP 20 min		HWP 40 min	
	M7	M9	M7	M9	M7	M9
Crystallinity (%)	28 (± 2)	31 (± 1)	32 (± 1)	34 (± 2)	39 (± 1)	41 (± 1)
LFD (nm)	2.4 (± 0.1)	2.6 (± 0.1)	2.6 (± 0.1)	2.7 (± 0.1)	3.0 (± 0.1)	3.1 (± 0.1)
LFAD (nm)	25 (±3)	27 (± 3)	39 (± 5)	31 (± 9)	37 (± 5)	74 (± 4)
β-O-4 bonds estimation (%)	48 (± 1)	49 (± 2)	40 (± 3)	43 (± 1)	36 (± 1)	32 (± 2)
$T_1\rho^H$ (ms)	18 (± 0)	22 (± 3)	33 (± 3)	37 (± 6)	45 (± 6)	50 (± 9)
T_{HH} (µs)	416 (± 32)	396 (± 61)	450 (± 73)	458 (± 100)	671 (± 121)	597 (± 122)

Lateral fiber dimension (LFD), lateral fiber aggregate dimension (LFAD), spin-lattice (proton relaxation) in the rotating frame ($T_1\rho^H$) and time of spin diffusion (T_{HH}). The analysis was realized on rehydrated CWR (20 % w/w) and the results are expressed as means of three repetitions with standard deviation into parentheses.

^{13}C CP/MAS NMR was also carried out to estimate the abundance of β-O-4 bonds representative of the entire lignin polymer **(53).** For this purpose, the intensities of the two broad signals at 152.4 ppm, which can be associated to the aromatic carbon atoms of lignin involved in β-O-4 bonds such as C-3 and C-5 of the S units, and 146.8 ppm, corresponding to the same carbons non-etherified, were determined **(Table 5)**. A depletion of the β-O-4 bonds

236 was detected with the application of the HWP and represented a decrease of about 17% and
237 25% for M7 and 12% and 35% for M9 for the 20 min and 40 min HWP, respectively. This
238 depletion induced by the acidification of the medium during pretreatment has also been
239 observed on other grasses species with HWP and dilute acid pretreatments **(26, 54)**.

240 Overall, HWP altered the ultrastructure of the lignin by breaking the β-O-4 bonds through the
241 acidic medium of the pretreatment. These modifications led to changes in the conformation of
242 the lignin surrounding the cellulose, which could also impact the ultrastructure of the cellulose.

243 2- Cellulose

244 Like for lignin, ^{13}C CP/MAS NMR was carried out to determine the impact of the HWP on the
245 ultrastructure of cellulose. For this, crystallinity and fibril dimensions, through lateral
246 dimension of the microfibrils (LFD) and of the microfibril aggregates (LFAD), were
247 determined by spectral deconvolution of the region of the cellulose C4 signals at around 80-91
248 ppm and presented in **Table 4**. LFD and LFAD was determined thanks to a conversion factor
249 of 0.57 nm per cellulose chain, and were schematically represented in **Figure 3 (55, 56)**.

250 **Fig. 3:** Schematic representation of raw cellulose fibril and cell wall organization.

251 Both raw CWR had a similar cellulose ultrastructure with average crystallinity, LFD and LFAD
252 values of around 26%, 2.5 nm and 30 nm, respectively. The crystallinity of the CWR increased
253 with the HWP severity. This relative increase of the crystallinity was linked to preferential
254 degradation/solubilization of amorphous cellulose during pretreatment by breaking intra-chain
255 hydrogen bonds. This solubilisation of amorphous cellulose is likely to explain part of the loss
256 of cellulose during the HWP shown above **(Table 1)**. A study comparing the effect of different
257 types of pretreatments on crystallinity showed that the acidity of the pretreatment medium was
258 directly related to the solubilization of amorphous cellulose **(57)**. During the HWP, the reaction

medium was gradually acidified with the increase of the pretreatment time, from a pH value of 4.4 at 20 min to 3.8 after a HWP 40 min **(Table 1)**. This acidification was negatively correlated (R^2 = -0.89) with the increasing loss of amorphous cellulose from about 13-17% with the HWP 20 min to 36-38% with the HWP 40 min for M9 and M7, respectively.

HWP also induced changes in the ultrastructure of the cellulose by slightly increasing the LFD. During the HWP, the loss of hemicelluloses (R^2 = 0.95) and amorphous cellulose (R^2 = 0.93) as well as the rearrangement of lignin, evidenced by the decrease in thioacidolysis yield (R^2 = 0.85) and β-O-4 bonds estimation (R^2 = 0.90), could be related with a loosening of the cellulose microfibrils and a possible swelling of the cellulose **(57, 58)**.

The increase in LFD was accompanied by an increase in LFAD. The increase in LFAD could be explained by the decrease in water-cellulose interactions (promoting cellulose-cellulose interactions) induced by heat, leading to an increase in aggregates size **(58-60)**. The HWP 40 min significantly modified the LFAD of genotype M9 compared to genotype M7. This difference suggests a strong hornification effect in M9 HWP 40 min due to an important co-crystallization of the cellulose induced by an efficient relocalization/modifications of the lignins and loss in hemicelluloses surrounding the cellulose and acting as spacer **(61-64)**.

The HWP induced changes in the cellulose architecture, leading to an increase in the dimension of the microfibrils and their aggregates. These modifications within the structure of the cellulose suggest an alteration of the cellulose interactions with its environment through the pretreatment.

3/ Modification of the interactions and the entanglement in the cell wall

A- Modification of cellulose interactions

Chemical analyses have shown that the HWP induced important changes in the composition of LB, in particular by removing a part of the hemicelluloses and by reorganizing the lignocellulosic components surrounding the cellulose, modifying its accessibility. Thus, the impact of HWP on the interactions and the accessibility of cellulose was investigated by solid-state NMR by studying the kinetic of polarization transfer **(Table 5)**.

First, the time constant $T_1\rho^H$ reported on the molecular organization surrounding the cellulose, longer is the $T_1\rho^H$, higher is the molecular order **(30)**. An increase of the $T_1\rho^H$ was observed for M7/M9 with the increase of the pretreatment time from 17/21 ms for raw CWR to 43/51 ms for the most severely pretreated CWR. This increase was positively correlated to crystallinity ($R^2 = 0.97$) and to the hemicelluloses loss ($R^2 = 0.95$), suggesting an increase in the molecular order surrounding the cellulose microfibrils after HWP due to the removal of amorphous components, cellulose and hemicelluloses **(Fig. 3)**. These results are in agreement with the studies by **(29)** and **(65)**, highlighting an increase of the $T_1\rho^H$ on HWP wheat and on dilute acid pretreated poplar, respectively.

This increase in molecular order was accompanied by an increase in the proton spin diffusion time (T_{HH}) after the HWP in both genotypes. T_{HH} reflects the diffusion of non-bounded protons magnetisation, which corresponds generally to the protons of water, close to cellulose **(66, 67)**. The increase of T_{HH} was positively correlated with the loss of hemicelluloses ($R^2 = 0.98$) and DiFA content ($R^2 = 0.84$), and with the content of Klason lignin ($R^2 = 0.91$) and negatively correlated to the proportion of S-units involved in ether bounds ($R^2 = -0.86$). This may suggest that the increase of the molecular order, related to the elimination of amorphous components, induces an increase of the spaces between the microfibrils favouring the accessibility of the water molecules and their interactions with cellulose.

The HWP has modified the ultrastructure of the cellulose but also its interactions with hemicelluloses/lignins making the microfibrils more accessible to water molecules. These modifications suggest changes in the porosity of the cell wall as well as in the accessible surface of the cellulose after HWP allowing it to increase the interactions of celluloses with water and therefore subsequently with hydrolytic enzymes.

B- Porosity and accessibility of cellulose

Simons' staining is a widely used technique to estimate the modifications induced by pretreatments on the structure and the environment of the cellulose through the analysis of the variation in the relative porosity as well as in the global accessible surface of the cellulose to cellulases **(68)**. Simons' staining is based on the adsorption of two contrasted dyes: DB1 for small-size pores with a hydrodynamic radius (r_H) around 1 nm and DY11 for pore sizes larger than the r_H of cellulases **(69, 70)**.

Fig. 4: Evolution of the total adsorbed dye and DY11/DB1 ratio of raw and pretreated samples.

Variation of the total accessible surface area (ASA) of cellulose was estimated from the total amount of dyes adsorbed **(fig. 4)**. No significant differences in the total amount of probes adsorbed was observed between the two genotypes, in accordance with their similar environment and similar cellulose structure. For both genotypes, an increase in the amount of dye adsorbed by the substrate was noted with increased HWP time, reflecting an increase of the ASA.

By measuring the total amount of adsorbed dyes and the DY11/DB1 ratio, the evolution of the relative amount and size of the pores of the CWR after HWP could be analysed **(71)**. Moreover, the variation of the ratio alone gives information on the variation of the specific surface area (SSA) of the cellulose accessible to cellulases. For raw genotypes, the close DY11/DB1 ratio

328 pointed out an akin SSA between the two genotypes. At a HWP time of 20 min, the evolution
329 of the ratio was different depending on genotype. For M7 with HWP 20 min, the increase in
330 the total adsorbed dye following by a slight increase in the DY11/DB1 ratio suggests the
331 generation of new "small" pores and a slight expansion of the existing pores allowing an
332 increase in the amount of adsorbed DB1 and DY11 respectively. In comparison, for M9, the
333 HWP 20 min resulted in a decrease in the DY11/DB1 ratio, and in an increase in the total
334 amount of adsorbed dye, which would imply only the generation of "small" pores. When the
335 HWP time was extended to 40 min, a significant increase in the DY11/DB1 ratio and in the
336 amount of the total adsorbed dye was detected for both genotypes in comparison to the raw
337 CWR. These results prove that the HWP 40 min mainly induce the expansion of the existing
338 pores allowing an increase in the adsorption of DY11. The DY11/DB1 ratio values were 2.93
339 and 1.97 times higher than those of the raw CWR M7 and M9, respectively, showing a clear
340 increase of SSA with this pretreatment time especially at M7.

341 Simons' staining has shown that the HWP increased the relative amount and the expansion of
342 pore and also the increase of SSA, two important parameters for the improvement of cellulose
343 hydrolysis (**23**). Here the increase in the SSA induced by HWP, was positively correlated with
344 the increase of the diffusion time T_{HH} ($R^2 = 0.96$) and the loss of hemicelluloses ($R^2 = 0.89$)
345 and amorphous cellulose ($R^2 = 0.88$). This correlation shows that a higher water-cellulose
346 interaction, related to a higher molecular order, allows an increase of the cellulases accessibility
347 to the cellulose. It was worth noting that the increase in the SSA was negatively correlated to
348 the yield of thioacidolysis ($R^2 = -0.96$), suggesting that the condensation of lignin induced by
349 HWP promotes cellulases accessibility to cellulose. Surprisingly, the increase in lignin content
350 was positively correlated with the DY11/DB1 ratio ($R^2 = 0.86$), indicating that lignin content
351 was not necessarily a contributor to recalcitrance and that changes in its structure could reduce
352 its negative impact on the cellulose accessibility. The effect of the HWP on the porosity of the

cell wall allowing an increase in the accessibility of the cellulose was investigated more precisely thanks to relaxometry analyses.

C- Water mobility:

Fig. 5: T_2 distribution for (a) M7 and (b) M9 samples with a water content of 20 % (w/w).

Change in water mobility after HWP is an important parameter to consider in order to obtain a better understanding of the effect of HWP on enzymatic hydrolysis. The changes in the water mobility were determined by NMR analyses of the relaxation times of water molecules in the CWR which can be associated with a range of pore sizes as previously explored **(26, 27, 71)**. The NMR analyses were carried out under controlled relative humidity: at 20 % (w/w) **(Fig. 5)**, similar to the measurements performed in solid state NMR, and 80 % (w/w) **(Fig. 6)**, similar to the humidity conditions during enzymatic hydrolysis.

At a humidity of 20%, two populations of water were detected. The HWP induced a decrease of the peak width (PW) for both genotypes, which indicates a homogenization of water constraint within the CWR after the HWP (**Additional file 2**). It was worth noting that the HWP led to the decrease of the amplitude of the water populations around 15 ms, which also suggests a homogenisation of the CWR after pretreatment through the domination of a major population. On the raw M9 CWR, the proportion of the water population (P_2) associated with T_2 around 19 ms was more important than M7, showing a higher water mobility disparity within this genotype.

Fig. 6: T_2 distribution for (a) M7 and (b) M9 samples with a water content of 80% (w/w).

In complement, the relaxation times of the different CWR were analysed at a relative humidity of 80% (w/w) in order to obtain more information on the effect of the HWP on the water redistribution and the porosity **(Fig. 6)**. An increase in the number of populations with higher

T_2 values were detected at 80% compared to 20% of relative humidity (2 populations at 20% versus 5 populations at 80%). These populations represent distinct environments, impacting differently the capacity of interaction and mobility of water molecules and probably resulting from the swelling of the cell wall with humidity. These water populations could be divided into three regions and related to different pore size ranges according to their T_2 values **(27)**.

The first region of relaxation time from 4 to 30 ms **(Fig. 6)** corresponds to "small" pore sizes between 5 and 15 nm (shaded area). This pore size range corresponds to the average enzyme size range **(72, 73)** and allows to provide more information on the mobility capacity of the enzymes within the lignocellulosic matrix after HWP. Within this first region, the water content of the population (P_2) with a T_2 around 8.4 ms was increased after HWP from 7.6% and 7.7% in the raw CWR to 16.8% and 18.3% with the 40 min HWP for CWR M7 and M9, respectively (**Additional file 3**). This increase can be explained either by the creation of new pores or by the compaction of larger domains during the HWP. The pretreatment also induced an increase in the inhomogeneity of this water content, apparent by an increase in the peak width (PW) after the HWP 40 min (**Additional file 3**). The water content associated with this pore size range was highly correlated to the modification of different chemical parameters such as hemicellulose loss ($R^2 = 0.98$), Klason lignin content ($R^2 = 0.98$), β-O-4 linkages estimation ($R^2 = -0.93$), and the molecular order ($R^2 = 0.96$). These results highlight that the loss of hemicelluloses as well as changes in the ultrastructure of lignin have a direct influence on the porosity of the CWR, promoting the accessibility and circulation of water after HWP.

In the second region of T_2 from 30 to 100 ms, corresponding to pore sizes between 15 and 40 nm, a decrease of the water content retained within this pore size range was detected for both genotypes. This observation can be explained by the redistribution of water by diffusion to the smaller size ranges. Indeed the total water proportion (P_2) inside the third region, with a T_2

400 higher to 100 ms, remained stable after HWP. Within this region, the mean T_2 of two water
401 pool environments increases with HWP from 210 ms to 271 ms and from 610 to 851 ms
402 respectively. Furthermore, a water transfer was observed from the water population with a T_2
403 of about 210 ms to the water population with a T_2 of about 600 ms. These observations suggest
404 that HWP induces a broadening of the large domains.

405 The HWP induces a modulation of the domains and promotes the creation of new domains
406 where the water is more constrained and which can be associated with pore sizes between 5
407 and 15 nm. This increase of the porosity, seen by NMR and Simons' staining, should favour
408 the mobility of enzymes and thus facilitate their catalytic activity.

409

410 **4/ Correlation of physico-chemical modifications induced by HWP on saccharification:**

411

412 In order to determine the impact of the physico-chemical modifications induced by the HWP
413 on enzymatic hydrolysis, and to identify the main factors contributing to recalcitrance,
414 correlation coefficients were calculated between the saccharification yields at 72 h and the
415 previously determined factors **(Fig. 7)**.

416

417 **Fig. 7:** Pearson's correlation coefficients between physico-chemical factors variations and
418 hydrolysis yield after 72h.

419

420 As shown, HWP led to an increase in the porosity of the cell wall, as indicated by the rise of
421 the water pool proportion associated with pore diameter in the range 5-15 nm, which includes
422 the average diameter of enzymes involved in hydrolysis. The increase in this pore size range
423 was strongly related to higher saccharification yield ($R^2 = 0.96$), which is in agreement with
424 the fact that 90% of the hydrolytic enzymes accessibility depends on the internal wall pores

425 **(9)**. The increase of the cell wall porosity was also supported by Simons' staining through the
426 increase of the adsorption of DY11 probe, which has a r_H close to that of cellulases. The
427 accessibility of cellulose estimated through ASA and more particularly for enzymes through
428 SSA was strongly correlated with the hydrolysis capacity of the CWR ($R^2 = 0.92$).

429 This increase in the porosity and accessibility to the cellulose was achieved by modifying the
430 intra- and inter-polymers interactions after the HWP. In fact, the analysis of cellulose
431 interactions by solid-state NMR showed that HWP induced an increase in the molecular order
432 surrounding the cellulose microfibrils ($T_1\rho^H$) (R^2 = 0.92) thanks to the decrease of the
433 interactions of cellulose with amorphous components such as hemicelluloses. This increase of
434 molecular order led to a loosening of the matrix and favoured the circulation/interaction of
435 water molecules (T_{HH}) (R^2 = 0.99) and then of enzymes. The loosening of the matrix
436 surrounding the cellulose microfibrils was in part due to the breaking of bonds involving FA
437 units, the major cross-linking agents in grasses **(74)**. Here the loss of DiFA, which binds GAX
438 together, was strongly correlated with saccharification yield ($R^2 = 0.96$), which is in agreement
439 with results found in the literature on grasses species such as sugarcane **(75),** *Phalaris aquatica*
440 and *Lolium* **(76)**. Interestingly, the loss of etherified FA was not strongly correlated with
441 saccharification yield (R^2 = 0.73), suggesting a higher importance of the destructuring of the
442 GAX-GAX network than GAX-lignin for bringing accessibility to enzymes.

443 In addition to hemicelluloses participation in the tight entanglement of the matrix,
444 hemicelluloses also have a protective role by covering cellulose microfibrils with multiple
445 layers and inserting themselves between them **(77)**. Indeed, hemicelluloses are bound to the
446 hydrophilic surfaces of cellulose through hydrogen bonds **(78)**, reducing the accessibility of
447 cellulose to cellulases **(63)**. Thus the loss of hemicelluloses induced by HWP contributed to
448 increase the accessibility of the enzyme within the matrix and also of the SSA as shown by the

449 strong correlation between hemicellulose loss and saccharification yield (R^2 = 0.99). During
450 HWP, the loss of hemicelluloses also led to an increase in the content of the lignin. Indeed, it
451 has been shown that the presence of lignin reduces the enzymatic hydrolysis potential due to
452 its role as a physical barrier, owing to the interactions with polysaccharides that reduce the
453 cellulose accessibility, and its non-specific interaction capacity with hydrolytic enzyme **(7, 79)**.
454 After HWP the increase of the lignin content showed a positive correlation with the
455 saccharification yield (R^2 = 0.93), suggesting that the lignin content was not directly related to
456 the recalcitrance of lignocellulose, as demonstrated in previous studies **(48, 80, 81)**. Thus,
457 chemical pretreatments aimed at eliminating lignin, such as oxidative alkaline or organosolv
458 pretreatments, are not necessarily the most suitable ways to improve saccharification **(26, 81)**.
459 Considering lignin organisation is a more relevant way to assess its impact on recalcitrance
460 than its content alone.

461 Our investigations highlighted that changes into the content and polymers interactions during
462 the HWP were associated with several modifications within the polymers ultrastructure and
463 more particularly of the lignin. First, HWP has been shown to increase the S/G ratio but it did
464 not significantly correlate with hydrolysis capacity (R^2=0.59), as already shown **(82)**. This
465 demonstrates that S/G ratio, determined by thioacidolysis, is not a predicting factor of
466 hydrolysis capacity **(83)** and that its impact is still unclear and depends on the LB species
467 considered. The decrease in the estimate of ether bonds (mainly β-O-4) as well as the increase
468 in the condensation state reflected by the thioacidolysis yield were both negatively correlated
469 with saccharification yield (R^2 = -0.93 and -0.86, respectively). These results suggest that the
470 condensed state of lignin after HWP might promote enzymatic deconstruction. This correlation
471 has already been observed **(82)** and may be explained by the variation in the lignin
472 conformation according to its inter-unit bonds (84). Indeed, it has been shown by molecular
473 modelling that a high concentration of β-O-4 bonds confers to lignin an extended conformation

favouring interactions with cellulose fibrils, thus forming a physical barrier and limiting access to cellulases **(84)**. The changes in the structure of lignin after HWP would decrease its protective role and promote the accessibility of cellulases to the cellulose microfibrils **(85)**. On the opposite, excessive condensation of lignin can be detrimental to enzymatic hydrolysis as it would promote strong aggregation of cellulose and therefore a decrease in its accessibility for cellulases **(64)**. This may be the case for the M9 HWP 40 min genotype, for which a strong aggregation of cellulose microfibrils has been observed together with a lower saccharification rate than the M7 HW 40 min genotype. This means that HWP severity should be balanced to favour enough lignin condensation promoting cellulose accessibility while limiting strong interactions. Fast and easy prediction of saccharification based on lignin organisation seems possible by measuring CWR autofluorescence (R^2 = -0.83), as previously observed for other pretreatments and LB species **(26, 49)**. It has been assumed previously **(86)** that lignin does not have a direct impact on the accessibility of enzymes but an indirect effect on hydrolysis capacity through its strong interaction with hemicelluloses. Our study confirms that the reshape of lignin organisation within the cell wall after HWP has a direct impact on the accessibility to the cellulose and the saccharification potential.

In addition, HWP had an impact on the ultrastructure of the cellulose by increasing its crystallinity and LFD. Crystallinity is often described as a limiting factor in enzymatic hydrolysis **(7, 87, 88)**. Here the increase in the crystallinity of the cellulose, induced by the loss of more hydrolysable amorphous cellulose during HWP, had no negative impact on the saccharification capacity of the CWR (R^2 = 0.93). The increase in LFD also showed a positive impact on saccharification (R^2 = 0.92). This observation could be associated with the swelling of the cellulose due to the opening of the matrix, leading to an increase of SSA.

Conclusion:

Our work has illustrated that hot water pretreatment (HWP) improved enzymatic hydrolysis by altering many interconnected factors ranging from the polymers' ultrastructure (bounds, crystallinity ...) to the organisation of the wall (mesoporosity). The loss of hemicelluloses and changes in polymers structural features induced by HWP leads to a significant reorganization of the lignocellulosic matrix. These modifications induce an increase in the specific surface area of the cellulose and a water redistribution allowing an increase in the accessibility of cellulases and an enhancement of the hydrolysis. Interestingly the environment and organization of lignin is thus more important to consider than its concentration to explain cellulose accessibility.

The multiscale combination of biochemical compositional techniques with solid-state NMR and NMR relaxometry analysis has been decisive to understand the interplay between polymers and recalcitrance of hot water pretreated LB. The same approach could be applied to other biomass species and other pretreatments in order to guide towards the best compromise between pretreatment severity and saccharification by elucidating the interactions between polymers.

Materials and Methods:

Plant materials:

Two maize genotypes F7025 (abbreviated as M7) and F98902 (as M9) were selected on the basis of preliminary composition results indicating differences in digestibility capacity, high and low digestibility, respectively **(89, 90)**. The genotypes were cultivated in the experimental plots of INRAE in Mauguio under irrigated conditions and harvested at the silage stage. The

internode under the main ear was isolated, dried and then cut into 2 cm fragments. The cell wall residue (CWR) was obtained after soluble components removal by an 8-hour ethanol extraction followed with a 48-hour water extraction.

Hot water pretreatment:

Hot water pretreatment (HWP) was performed on 2 cm-half-fragments of CWR maize in mineralization bombs equipped with Teflon cups (Parr, USA). Each half-fragment was pretreated with a volume of deionized water adjusted for a ratio of 1:30 (v/w) **(26)**, in an oil bath at a constant temperature of 180 °C during two variable durations of 20 and 40 min. CWR were cooled in ice and then washed with 50% ethanol solution and deionized water until the soluble components were completely removed. The pretreatment parameters were chosen on the basis of previous experiments to preserve the structure of the CWR for microscopy imaging **(26, 31, 91)**.

The consolidated severity factor (CSF) of these pretreatments was calculated according to Eq.(1) **(92)**:

$$CSF = log\left[t \times exp\left(\frac{T_i - T_{ref}}{14.75}\right)\right] \textbf{ (Eq. 1)}$$

Where *t* represents the time of pretreatment, T_i the temperature of the pretreatment (180 °C) and T_{ref} the reference temperature of 100 °C.

Compositional analyses of CWR:

For the global biochemical and physico-chemical analysis, the CWR were ground with an ultra centrifugal mill (ZM200, Retsch, Germany) to an average granulometry of 1 mm.

Polysaccharides analysis:

The monomeric sugars content were quantified by HPAEC-PAD after a two-step H_2SO_4 hydrolysis as described previously **(93)**.

545 *Ferulic acid and p-coumaric acid content:*

546 Mild and severe alkaline hydrolysis:

547 The esterified and etherified contents of ferulic acid and *p*-coumaric acid was determined by
548 alkaline hydrolysis at two different severities. Mild alkaline hydrolysis was applied on 10 mg
549 of CWR with 1 mL of NaOH at 1 M during one night at room temperature. Severe alkaline
550 hydrolysis was realized on 10 mg of powder with 2 mL of NaOH at 4 M during 2 hours at 170
551 °C. The hydrolysate was subsequently acidified to pH < 3 (with 6 M HCl), centrifuged at 12,000
552 g for 10 min, purified into on a solid-phase extraction cartridge (Waters Sep-pack t18, USA)
553 with 0.1% HCOOH and then the phenolic compounds were eluted with methanol. The phenolic
554 compounds were analyzed on HPLC according to a published method **(94)**.

555 Ferulic acid and *p*-coumaric acid were quantified using *o*-coumaric acid as an internal standard
556 and *o*-coumaric acid, ferulic acid and *p*-coumaric acid as a solution standard.

557 The content of esterified hydroxycinnamic acids was determined by the amount of ferulic and
558 *p*-coumaric acid released during mild alkaline hydrolysis. Etherified ferulic acid content was
559 calculated by the difference between the amount of esterified ferulic acid released by mild and
560 the total amount of ferulic acid released by severe alkaline hydrolysis.

561 *Acetyl content:*

562 An alkaline hydrolysis was carried out on 5 mg of CWR with 1 M NaOH at 4 °C during 30
563 min. After the stabilization of the pH at 8 with 1 M HCl, the acetyl content was quantified with
564 a commercial acetic acid kit (BiosenTec, Portet-sur-Garonne, France).

565

566 *Klason lignin content:*

567 200 mg of CWR (M) were hydrolyzed with 2 mL of 12 M sulfuric acid solution at room
568 temperature for 2 h. The hydrolysate was diluted with deionized water to achieve the acid
569 sulfuric concentration to 2 M and the mixture was incubated 3 h at 300 °C with an agitation of

500 rpm. The solid residues were filtered and washed with deionized water, dried at 100 ° C for 20 h and then weighted (W_1). Finally, the sample was calcined at 600 °C for 3h30 and the weight was noted (W_2) **(95)**.

The total Klason lignin content was calculated according to Eq. 2:

$$KL(\%) = \frac{(W_1 - W_2)}{M} \times 100 \quad \textbf{(Eq. 2)}$$

Thioacidolysis:

The monomeric composition of the ether-linked lignin fraction was determined by thioacidolysis as described by **(96)**. The reaction reagent composed of dioxane/boron trifluoride etherate/ethanethiol (87.5/2.5/10, v/v/v) was prepared and 1 mL was added to 10 mg of CWR with 1 mL of internal standard tetracosane at 0.25 mg.mL^{-1}, then the mixture was heated at 100 °C for 4 h. The phenolic compounds were extracted from the reaction medium with the addition of 3 × 25 mL of dichloromethane and concentrated by evaporation. The monomeric units of the lignin were then silylated to be quantified by GC equipped with a fused silica capillary DB1 column (30 m × 0.3 mm) (J&W Scientific, USA) and flame ionisation detector.

FTIR analysis:

Pellets were prepared from 2 mg of CWR in powder mixed with 300 mg of KBr then analyzed in MIR on a Nicolet 6700 Thermo Electron FTIR spectrometer with a KBr separator and a DTGS KBr detector. Spectra were recorded three times in the range 4000 – 400 cm^{-1} with a resolution of 4 cm^{-1} and 16 scans per sample. The baseline of the spectra was corrected using the Omnic software and then normalized by area by applying a correction factor of $\frac{1000}{A_{2000-800\,cm-1}}$, where $A_{2000-800}$ cm^{-1} was the area of the spectra between 2000 - 800 cm^{-1}.

3D fluorescence maps:

3D fluorescence maps on raw and hot-water pretreated CWR were performed using a JASCO FP8300 spectrofluorometer (Japan). The 3D maps were acquired with excitation wavelengths scanning from 300 to 550 nm, with a wavelength increment of 2 nm, emission wavelengths scanning from 350 to 600 nm, with wavelength increment of 0.2 nm. The sensitivity was set to 500 V. The 3D maps were analyzed with Jasco SpectraManager software.

Simons' staining:

The accessible surface area of the cellulose and the relative porosity of the LB were determined by Simons' staining procedure as previously described **(97, 98)**. Direct Blue 1 (DB1) was purchased from Pylam Products Company (USA). Direct Yellow 11 (DY11) was obtained from Sigma-Aldrich (USA). DY11 was purified with 100 kDa (molecular weight cut-off) polyethersulfone membranes, and only the supernatant, with a MW greater than 100 kDa, was used. DB1 and DY11 were prepared to yield 10 mg/mL by adding deionised water. 10 mg of substrate were added into 2 mL tubes and mixed with 0.1 mL of phosphate buffer (140 mM NaCl, 0.3 M phosphate, pH 6.0), an increasing volume of both dyes (0.025, 0.05, 0.75, 0.1, 0.15 and 0.2 mL) followed by the addition of deionized water to adjust the final volume to1 mL. The tubes were incubated at 70 °C for 6 h with an agitation of 300 rpm. After the incubation, the tubes were centrifuged at 12,000 g for 5 min, then the absorbance of the supernatant was analysed after dilution to the 100^{th} with a spectrophotometer (UV-3100 PC, VWR, USA) at 430 and 600 nm. The amount of dye adsorbed onto the biomass was determined using the difference between the concentration of the initial added dye and the concentration of the dye in the supernatant, as described by Alam et al. **(69)**.

^{13}C Solid-state NMR:

Approximately 80 mg of each CWR were rehydrated to 24-26% (w/w) with ultra-pure water. All the analyses were carried out as biological triplicates. The solid-state NMR spectra were carried out on a Bruker Avance III 400 MHz spectrometer operating at a carbon frequency of 100.62 MHz. A double resonance $^{1}H/X$ CP/MAS 4 mm probe coupled with a high power level amplifier was used for ^{13}C CP/MAS experiment. The magic angle spinning (MAS) rate was set at 12 kHz and each acquisition was acquired at ambient temperature (25 °C). The experiment was conducted under a 90° proton pulse of 2.6 ± 0.1 µs, a contact time of 1.5 ms and a 10 s recycling time. Each spectrum was the result of the accumulation of 2048 scans. Chemical shifts were calibrated using glycine as external reference, assigning the carbonyl at 176.03 ppm.

The chemical shifts, half width and area of peak of samples were determined using a least-squares fitting method with the Peakfit® software (Systat Software Inc., USA).

According to the method of Larsson et al. **(99)**, the cellulose crystallinity was calculated from deconvolution of cellulose C_4 peaks in the region of 80-91 ppm. This method is performed thanks to the use of three Lorentzian peaks corresponding to cellulose Cr(Iα) (88.1 ppm), cellulose Cr(Iα+β) (86.8 ppm) and cellulose Cr(Iβ) (86.2 ppm). An additional Gaussian peak associated with the para-crystalline (PCr) contribution (87.9 ppm) was used. Three peaks were used in the amorphous C4 region, two Gaussian peaks corresponding to the accessible surface cellulose C4 (82.9 and 84.1 ppm) and another one for the inaccessible surface C4 (83.4 ppm). The proportion of crystalline cellulose was determined by dividing the sum peak area of four crystalline cellulose C_4 peaks by those of seven cellulose C_4 peaks. Assuming the cross section of cellulose microfiber is square and all amorphous cellulose is attached on the fiber surface, the lateral fiber dimension (LFD) and the lateral dimensions of the fibril aggregates (LFAD) were also estimated. The cellulosic chains width was set at 0.57 nm **(100)**.

The molecular dynamic of samples was further characterized by varying contact time (τ) from 10 µs to 9000 µs. Twenty CP/MAS spectra were recorded with an accumulation of 512 scans per contact time. The evolution of carbon peak area (C_4 of crystalline cellulose and O-CH_3 of pectin methyl ester) between different groups was fitted according to Eq. 3 **(101)**:

$$I(\tau) = I_0 e^{-\tau/T_{1\rho}^H} * \left\{1 - \lambda e^{-\tau/T_{HH}} - (1-\lambda) e^{-3\tau/T_{2HH}} e^{-\tau^2/2T_{CH}^2}\right\} \quad \textbf{(Eq. 3)}$$

where $I(\tau)$ is the carbon peak area (C_4 of crystalline cellulose and O-CH_3 of pectin methyl ester) according to the contact time (τ), I_0 is the maximum carbon signal intensity (associated with the optimal contact time), λ is a parameter that depends on the number of protons (n) carried by carbons (λ=1/(n+1)), $T_{CH}$is the mean dipolar coupling between carbon and covalently linked proton, $T_1\rho^H$ is the spin-lattice proton relaxation time, T_{HH} is the spin diffusion time between two nearby protons.

Time-Domain NMR:

These interactions can be related to the porosity of the system. 80 mg of each CWR were analysed at two hydration levels, about 20% (low) and 80% (high) (w/w). Transverse relaxation (T_2) was measured at 4 °C on a Bruker Minispec mq20 (0.47 T), equipped with a thermostated ^{1}H probe, using the Carr-Purcell-Meiboom-Gill (CPMG) pulse sequence. For low hydration, echo time was 80 µs, 400 even echoes were collected and 384 scans were acquired with a recycle delay of 3 s. For high hydration, echo time was 1 ms, 2000 even echoes were collected and 128 scans were acquired with a recycle delay of 7 s. An inverse Laplace transformation (ILT) was applied **(102)** to convert the relaxation signal into a continuous distribution of the relaxation components **(26)**.

Enzymatic saccharification:

663 The enzymatic saccharification was performed with the commercial enzymatic cocktail Cellic
664 CTec 2 (Novozymes, Denmark) containing cellulase and xylanase activity of 205 FPU.mL^{-1}
665 and 9068 UI.mL^{-1}, respectively. Raw and pretreated milled CWR (20 mg) were added to 1 mL
666 of 50 mM acetate buffer pH 5.2 with 0.15 mg.mL^{-1} of tetracycline as antibiotic, 0.04 mg.mL^{-1}
667 cycloheximide as antifungal agent, into 2 mL tubes. The micro-reactors (powder and medium)
668 were pre-incubated for 20 min at 50 °C, then Cellic CTec 2 cocktail was loaded at a final
669 concentration of 30 FPU.g^{-1} of biomass and the mixtures were incubated at 50 °C with an
670 agitation of 300 rpm.

671 Aliquots of 12 µL were taken at different hydrolysis timepoints: 0, 0.5, 1, 2, 4, 8, 24, 48, 72 h.
672 The aliquots were heated at 100 °C for 2 min, and then centrifuged at 12,000 g for 5 min. The
673 reducing sugars hydrolysed over time were determined via DNS assay.

674 *Determination of reducing sugars by DNS assay:*

675 The 3,5-Dinitrosalicylic acid (DNS) reagent was prepared according to the protocol established
676 by **(103)**. In 1.5 mL tubes, 60 µL of aliquot diluted 10 times were mixed with 120 µL of DNS
677 and heated at 100 °C for 10 min. The reducing sugars contained in the aliquots were determined
678 with a spectrophotometer (UV–3100 PC, VWR, USA) at 540 nm after diluting 100 µL of
679 solution in 1.25 mL of deionized water. A standard curve of glucose was used to calculate the
680 glucose reducing sugar equivalent in the different CWR.
681 The initial reaction rate was calculated as the tangent to the hydrolysis curve, converted sugars
682 (g.L^{-1}) plotted against reaction time (hours), at the initial time and was expressed in g.L^{-1}.h^{-1}.

683 Correlation analysis:

684 Pearson's simple correlation coefficient (R^2) and the Pearson correlation matrix was calculated
685 with SigmaPlot 12.0 (Systat Software Inc., USA). According to the population size, for pairs

686 of variables with *p* values lower than 0.050, there was a significant relationship between the
687 two variables.

688

689 **Abbreviations:**

690 ASA: accessible surface area;

691 CP/MAS NMR: cross polarization/ magic angle spinning nuclear magnetic resonance;

692 CPMG: Carr-Purcell-Meiboom-Gill;

693 Cr: crystalline region of cellulose;

694 CSF: consolidated severity factor;

695 CWR: cell wall residue;

696 DB1: direct blue 1;

697 DiFAe: esterified diferulic acid;

698 DNS: 3,5-Dinitrosalicylic acid;

699 DY11: direct yellow 11;

700 FA: ferulic acid;

701 FTIR: fourier-transform infrared spectroscopy;

702 GAX: glucuronoarabinoxylans;

703 HPAEC-PAD: high-performance anion-exchange chromatography with pulsed amperometric
704 detection;

705 HWP: hot water pretreatment;

706 ILT: Laplace transformation;

707 KL: klason lignin;

708 LB: lignocellulosic biomass;

709 LCC: lignin-carbohydrate complex;

LFD: lateral fiber dimension

LFAD: lateral fibril aggregates dimension;

M7: F7025 genotype;

M9: F98902 genotype;

P_2: peak proportion;

p-CA: p-coumaric acid;

PCr: para-cristalline region of cellulose;

PW: peak width;

R^2: Pearson's simple correlation coefficient;

r_H: hydrodynamic radii;

S/G: syringyl/guaiacyl lignin units

SSA: specific surface area;

T_2: relaxation time;

$T_1\rho^H$: spin-lattice proton relaxation time;

T_{HH}: spin diffusion time between two nearby protons;

VCT: variation time contact;

Ethics approval and consent to participate:

Not applicable.

Consent for publication:

Not applicable.

Availability of data and materials:

All data generated or analysed during this study are included in this published article and its supplementary information files.

Competing interests:

The authors declare that they have no competing interests

Funding:

Funding of Amandine Leroy PhD was provided by Région Grand-Est/Grand Reims.

Authors' contributions:

All authors contributed to this work via scientific discussion. AL planned and performed experiments, data analysis and drafted the manuscript. XF and LF performed the solid-state and low-field NMR measurements and interpretation. VM performed the severe alkaline hydrolysis analyses and analysed the corresponding data. FG and GP designed the study, coordinated the experiments and drafted the manuscript. All authors read and approved the final manuscript.

Acknowledgements:

The authors would like to thank some members of the FARE staff: David Crônier for his help in performing Klason lignin and thioacidolysis analyses, François Gaudard and Anouck Habrant for their help in performing in HPAEC-PAD analysis; and some members of the BIA staff: Audrey Geairon, Sylviane Daniel and Luc Saulnier for their help in performing hydroxycinnamic acids analysis.

References:

1. Ubando AT, Felix CB, Chen W-H. Biorefineries in circular bioeconomy: A comprehensive review. Bioresource technology. 2020;299:122585.

2. Baruah J, Nath BK, Sharma R, Kumar S, Deka RC, Baruah DC, et al. Recent Trends in the Pretreatment of Lignocellulosic Biomass for Value-Added Products. Frontiers in Energy Research. 2018;6(141).

757 3. Yang B, Tao L, Wyman CE. Strengths, challenges, and opportunities for hydrothermal
758 pretreatment in lignocellulosic biorefineries. Biofuels, Bioproducts and Biorefining.
759 2018;12(1):125-38.
760 4. Vu HP, Nguyen LN, Vu MT, Johir MAH, McLaughlan R, Nghiem LD. A
761 comprehensive review on the framework to valorise lignocellulosic biomass as biorefinery
762 feedstocks. Science of The Total Environment. 2020;743:140630.
763 5. Duque A, Alvarez C, Domenech P, Manzanares P, Moreno AD. Advanced Bioethanol
764 Production: From Novel Raw Materials to Integrated Biorefineries. Processes. 2021;9(2).
765 6. Zhao X, Zhang L, Liu D. Biomass recalcitrance. Part I: the chemical compositions and
766 physical structures affecting the enzymatic hydrolysis of lignocellulose. Biofuels, Bioproducts
767 and Biorefining. 2012;6(4):465-82.
768 7. Zoghlami A, Paes G. Lignocellulosic Biomass: Understanding Recalcitrance and
769 Predicting Hydrolysis. Front Chem. 2019;7.
770 8. Zhao X, Zhang L, Liu D. Biomass recalcitrance. Part II: Fundamentals of different pre-
771 treatments to increase the enzymatic digestibility of lignocellulose. Biofuels, Bioproducts and
772 Biorefining. 2012;6(5):561-79.
773 9. Baig KS. Interaction of enzymes with lignocellulosic materials: causes, mechanism and
774 influencing factors. Bioresources and bioprocessing. 2020;7(1):19.
775 10. Alvira P, Tomas-Pejo E, Ballesteros M, Negro MJ. Pretreatment technologies for an
776 efficient bioethanol production process based on enzymatic hydrolysis: A review. Bioresource
777 technology. 2010;101(13):4851-61.
778 11. Kumar B, Bhardwaj N, Agrawal K, Chaturvedi V, Verma P. Current perspective on
779 pretreatment technologies using lignocellulosic biomass: An emerging biorefinery concept.
780 Fuel Processing Technology. 2020;199:106244.

781 12. Hassan SS, Williams GA, Jaiswal AK. Emerging technologies for the pretreatment of
782 lignocellulosic biomass. Bioresource technology. 2018;262:310-8.
783 13. Kumar AK, Sharma S. Recent updates on different methods of pretreatment of
784 lignocellulosic feedstocks: a review. Bioresources and bioprocessing. 2017;4(1):7.
785 14. Liao Y, de Beeck BO, Thielemans K, Ennaert T, Snelders J, Dusselier M, et al. The
786 role of pretreatment in the catalytic valorization of cellulose. Molecular Catalysis.
787 2020;487:110883.
788 15. Batista G, Souza RBA, Pratto B, dos Santos-Rocha MSR, Cruz AJG. Effect of severity
789 factor on the hydrothermal pretreatment of sugarcane straw. Bioresource technology.
790 2019;275:321-7.
791 16. Rios-González LJ, Morales-Martínez TK, Rodríguez-Flores MF, Rodríguez-De la
792 Garza JA, Castillo-Quiroz D, Castro-Montoya AJ, et al. Autohydrolysis pretreatment
793 assessment in ethanol production from agave bagasse. Bioresource technology. 2017;242:184-
794 90.
795 17. Tan L, Liu Z, Zhang T, Wang Z, Liu T. Enhanced enzymatic digestibility of poplar
796 wood by quick hydrothermal treatment. Bioresource technology. 2020;302:122795.
797 18. Fan S, Zhang P, Li F, Jin S, Wang S, Zhou S. A review of lignocellulose change during
798 hydrothermal pretreatment for bioenergy production2016. 2799-809 p.
799 19. Takada M, Rabemanolontsoa H, Minami E, Saka S. Characterization of lignin-derived
800 products from various lignocellulosics as treated by semi-flow hot-compressed water. Journal
801 of Wood Science. 2018;64(6):802-9.
802 20. Zhuang X, Wang W, Yu Q, Qi W, Wang Q, Tan X, et al. Liquid hot water pretreatment
803 of lignocellulosic biomass for bioethanol production accompanying with high valuable
804 products. Bioresource technology. 2016;199:68-75.

21. Stone JE, Scallan AM. Effect of component removal upon the porous structure of the cell wall of wood. Journal of Polymer Science Part C: Polymer Symposia. 1965;11(1):13-25.

22. Driemeier C, Oliveira MM, Curvelo AAS. Lignin contributions to the nanoscale porosity of raw and treated lignocelluloses as observed by calorimetric thermoporometry. Industrial Crops and Products. 2016;82:114-7.

23. Zhang H, Li J, Huang G, Yang Z, Han L. Understanding the synergistic effect and the main factors influencing the enzymatic hydrolyzability of corn stover at low enzyme loading by hydrothermal and/or ultrafine grinding pretreatment. Bioresource technology. 2018;264:327-34.

24. Wang QQ, He Z, Zhu Z, Zhang Y-HP, Ni Y, Luo XL, et al. Evaluations of cellulose accessibilities of lignocelluloses by solute exclusion and protein adsorption techniques. Biotechnology and Bioengineering. 2012;109(2):381-9.

25. Meng X, Wells T, Sun Q, Huang F, Ragauskas A. Insights into the effect of dilute acid, hot water or alkaline pretreatment on the cellulose accessible surface area and the overall porosity of Populus. Green Chemistry. 2015;17:4239-46.

26. Herbaut M, Zoghlami A, Habrant A, Falourd X, Foucat L, Chabbert B, et al. Multimodal analysis of pretreated biomass species highlights generic markers of lignocellulose recalcitrance. Biotechnol Biofuels. 2018;11:52.

27. Barron C, Devaux M-F, Foucat L, Falourd X, Looten R, Joseph-Aime M, et al. Enzymatic degradation of maize shoots: monitoring of chemical and physical changes reveals different saccharification behaviors. Biotechnology for Biofuels. 2021;14(1):1.

28. Chandra RP, Ewanick SM, Chung PA, Au-Yeung K, Rio LD, Mabee W, et al. Comparison of methods to assess the enzyme accessibility and hydrolysis of pretreated lignocellulosic substrates. Biotechnology Letters. 2009;31(8):1217-22.

29. Habets S, de Wild PJ, Huijgen WJJ, van Eck ERH. The influence of thermochemical treatments on the lignocellulosic structure of wheat straw as studied by natural abundance 13C NMR. Bioresource technology. 2013;146:585-90.

30. Lahaye M, Falourd X, Laillet B, Le Gall S. Cellulose, pectin and water in cell walls determine apple flesh viscoelastic mechanical properties. Carbohydrate Polymers. 2020;232:115768.

31. Li X, Lu J, Zhao J, Qu Y. Characteristics of corn stover pretreated with liquid hot water and fed-batch semi-simultaneous saccharification and fermentation for bioethanol production. PLoS One. 2014;9(4):e95455.

32. Bianquini TS, Florencio C, Henrique dos Santos Garcia R, Colnago LA, Ceccato-Antonini SR, Carmo M, et al. Time domain NMR spectroscopy as a fast method for probing the efficiency of biomass pretreatments for second generation ethanol production. Biomass and Bioenergy. 2020;142:105734.

33. Robert P, Marquis M, Barron C, Guillon F, Saulnier L. FT-IR Investigation of Cell Wall Polysaccharides from Cereal Grains. Arabinoxylan Infrared Assignment. Journal of agricultural and food chemistry. 2005;53(18):7014-8.

34. Kačuráková M, Capek P, Sasinková V, Wellner N, Ebringerová A. FT-IR study of plant cell wall model compounds: pectic polysaccharides and hemicelluloses. Carbohydrate Polymers. 2000;43(2):195-203.

35. Devaux M-F, Jamme F, André W, Bouchet B, Alvarado C, Durand S, et al. Synchrotron Time-Lapse Imaging of Lignocellulosic Biomass Hydrolysis: Tracking Enzyme Localization by Protein Autofluorescence and Biochemical Modification of Cell Walls by Microfluidic Infrared Microspectroscopy. Frontiers in plant science. 2018;9(200).

852 36. Li C, Knierim B, Manisseri C, Arora R, Scheller HV, Auer M, et al. Comparison of
853 dilute acid and ionic liquid pretreatment of switchgrass: Biomass recalcitrance, delignification
854 and enzymatic saccharification. Bioresource technology. 2010;101(13):4900-6.
855 37. Chazal R, Robert P, Durand S, Devaux MF, Saulnier L, Lapierre C, et al. Investigating
856 lignin key features in maize lignocelluloses using infrared spectroscopy. Applied spectroscopy.
857 2014;68(12):1342-7.
858 38. Garrote G, Domínguez H, Parajó JC. Hydrothermal processing of lignocellulosic
859 materials. Holz als Roh- und Werkstoff. 1999;57(3):191-202.
860 39. Mosier N, Wyman C, Dale B, Elander R, Lee YY, Holtzapple M, et al. Features of
861 promising technologies for pretreatment of lignocellulosic biomass. Bioresource technology.
862 2005;96(6):673-86.
863 40. Shinde S, Meng X, Kumar R, Ragauskas A. Recent advances in understanding the
864 pseudo-lignin formation in a lignocellulosic biorefinery. Green Chemistry. 2018;20:2192-205.
865 41. Trajano HL, Engle NL, Foston M, Ragauskas AJ, Tschaplinski TJ, Wyman CE. The
866 fate of lignin during hydrothermal pretreatment. Biotechnology for Biofuels. 2013;6(1):110.
867 42. Saulnier L, Crépeau M-J, Lahaye M, Thibault J-F, Garcia-Conesa MT, Kroon PA, et
868 al. Isolation and structural determination of two 5,5′-diferuloyl oligosaccharides indicate that
869 maize heteroxylans are covalently cross-linked by oxidatively coupled ferulates. Carbohydrate
870 Research. 1999;320(1):82-92.
871 43. Hatfield RD, Rancour DM, Marita JM. Grass Cell Walls: A Story of Cross-Linking.
872 Frontiers in plant science. 2017;7(2056).
873 44. Ralph J. Hydroxycinnamates in lignification. Phytochemistry Reviews. 2010;9(1):65-
874 83.
875 45. Iiyama K, Lam TBT, Stone BA. Covalent Cross-Links in the Cell Wall. Plant
876 physiology. 1994;104(2):315-20.

877 46. Tarasov D, Leitch M, Fatehi P. Lignin-carbohydrate complexes: properties,
878 applications, analyses, and methods of extraction: a review. Biotechnology for biofuels.
879 2018;11:269-.
880 47. Grabber JH, Mertens DR, Kim H, Funk C, Lu F, Ralph J. Cell wall fermentation
881 kinetics are impacted more by lignin content and ferulate cross-linking than by lignin
882 composition. Journal of the Science of Food and Agriculture. 2009;89(1):122-9.
883 48. Demartini JD, Pattathil S, Avci U, Szekalski K, Mazumder K, Hahn MG, et al.
884 Application of monoclonal antibodies to investigate plant cell wall deconstruction for biofuels
885 production. Energy and Environmental Science. 2011;4:4332-9.
886 49. Auxenfans T, Terryn C, Paës G. Seeing biomass recalcitrance through fluorescence.
887 Scientific Reports. 2017;7.
888 50. Catherine L, Pollet B, Monties B, Rolando C. Thioacidolysis of Spruce Lignin: GC-
889 MS Analysis of the Main Dimers Recovered After Raney Nickel Desulphuration.
890 Holzforschung. 1991;45:61-8.
891 51. Takeda Y, Tobimatsu Y, Yamamura M, Takano T, Sakamoto M, Umezawa T.
892 Comparative evaluations of lignocellulose reactivity and usability in transgenic rice plants with
893 altered lignin composition. Journal of Wood Science. 2019;65(1):6.
894 52. Miyamoto T, Mihashi A, Yamamura M, Tobimatsu Y, Suzuki S, Takada R, et al.
895 Comparative analysis of lignin chemical structures of sugarcane bagasse pretreated by alkaline,
896 hydrothermal, and dilute sulfuric acid methods. Industrial Crops and Products. 2018;121:124-
897 31.
898 53. Bardet M, Gerbaud G, Giffard M, Doan C, Hediger S, Pape L. 13C high-resolution
899 solid-state NMR for structural elucidation of archaeological woods. Progress in Nuclear
900 Magnetic Resonance Spectroscopy. 2009;55:199-214.

54. Auxenfans T, Crônier D, Chabbert B, Paës G. Understanding the structural and chemical changes of plant biomass following steam explosion pretreatment. Biotechnology for biofuels. 2017;10:36-.

55. Sugiyama J, Vuong R, Chanzy H. Electron diffraction study on the two crystalline phases occurring in native cellulose from an algal cell wall. Macromolecules. 1991;24(14):4168-75.

56. Villares A, Moreau C, Bennati-Granier C, Garajova S, Foucat L, Falourd X, et al. Lytic polysaccharide monooxygenases disrupt the cellulose fibers structure. Scientific Reports. 2017;7(1):40262.

57. Sun Q, Foston M, Sawada D, Pingali SV, O'Neill HM, Li H, et al. Comparison of changes in cellulose ultrastructure during different pretreatments of poplar. Cellulose. 2014;21(4):2419-31.

58. Foston M, Ragauskas AJ. Changes in lignocellulosic supramolecular and ultrastructure during dilute acid pretreatment of Populus and switchgrass. Biomass and Bioenergy. 2010;34(12):1885-95.

59. Silveira RL, Stoyanov SR, Kovalenko A, Skaf MS. Cellulose Aggregation under Hydrothermal Pretreatment Conditions. Biomacromolecules. 2016;17(8):2582-90.

60. Yao K, Wu Q, An R, Meng W, Ding M, Li B, et al. Hydrothermal pretreatment for deconstruction of plant cell wall: Part II. Effect on cellulose structure and bioconversion. AIChE Journal. 2018;64(6):1954-64.

61. Sun Q, Foston M, Meng X, Sawada D, Pingali SV, O'Neill HM, et al. Effect of lignin content on changes occurring in poplar cellulose ultrastructure during dilute acid pretreatment. Biotechnology for Biofuels. 2014;7(1):150.

62. Salmén L, Stevanic JS. Effect of drying conditions on cellulose microfibril aggregation and "hornification". Cellulose. 2018;25(11):6333-44.

926 63. Pu Y, Hu F, Huang F, Davison BH, Ragauskas AJ. Assessing the molecular structure
927 basis for biomass recalcitrance during dilute acid and hydrothermal pretreatments.
928 Biotechnology for Biofuels. 2013;6(1):15.
929 64. Ishizawa CI, Jeoh T, Adney WS, Himmel ME, Johnson DK, Davis MF. Can
930 delignification decrease cellulose digestibility in acid pretreated corn stover? Cellulose.
931 2009;16(4):677-86.
932 65. Kohn B, Davis M, Maciel GE. In situ Study of Dilute H2SO4 Pretreatment of 13C-
933 Enriched Poplar Wood, Using 13C NMR. Energy & Fuels. 2011;25(5):2301-13.
934 66. Jarvis MC, Fenwick KM, Apperley DC. Cross-polarisation kinetics and proton NMR
935 relaxation in polymers of Citrus cell walls. Carbohydrate Research. 1996;288:1-14.
936 67. Paris M, Bizot H, Emery J, Buzaré JY, Buléon A. NMR local range investigations in
937 amorphous starchy substrates: II-Dynamical heterogeneity probed by 1H/13C magnetization
938 transfer and 2D WISE solid state NMR. International Journal of Biological Macromolecules.
939 2001;29(2):137-43.
940 68. Chandra R, Ewanick S, Hsieh C, Saddler JN. The characterization of pretreated
941 lignocellulosic substrates prior to enzymatic hydrolysis, part 1: a modified Simons' staining
942 technique. Biotechnol Prog. 2008;24(5):1178-85.
943 69. Alam A, Zhang R, Liu P, Huang J, Wang Y, Hu Z, et al. A finalized determinant for
944 complete lignocellulose enzymatic saccharification potential to maximize bioethanol
945 production in bioenergy Miscanthus. Biotechnology for Biofuels. 2019;12(1):99.
946 70. Sun D, Alam A, Tu Y, Zhou S, Wang Y, Xia T, et al. Steam-exploded biomass
947 saccharification is predominately affected by lignocellulose porosity and largely enhanced by
948 Tween-80 in Miscanthus. Bioresource technology. 2017;239:74-81.

949 71. Meng X, Foston M, Leisen J, DeMartini J, Wyman CE, Ragauskas AJ. Determination
950 of porosity of lignocellulosic biomass before and after pretreatment by using Simons' stain and
951 NMR techniques. Bioresource technology. 2013;144:467-76.
952 72. Grethlein HE. The Effect of Pore Size Distribution on the Rate of Enzymatic Hydrolysis
953 of Cellulosic Substrates. Bio/Technology. 1985;3(2):155-60.
954 73. Fong M, Berrin J-G, Paës G. Investigation of the binding properties of a multi-modular
955 GH45 cellulase using bioinspired model assemblies. Biotechnology for biofuels. 2016;9:12-.
956 74. Hatfield RD, Ralph J, Grabber JH. Cell wall cross-linking by ferulates and diferulates
957 in grasses. Journal of the Science of Food and Agriculture. 1999;79(3):403-7.
958 75. Lam TB-T, Iiyama K, Stone BA. Hot alkali-labile linkages in the walls of the forage
959 grass Phalaris aquatica and Lolium perenne and their relation to in vitro wall digestibility.
960 Phytochemistry. 2003;64(2):603-7.
961 76. Siqueira G, Milagres AMF, Carvalho W, Koch G, Ferraz A. Topochemical distribution
962 of lignin and hydroxycinnamic acids in sugar-cane cell walls and its correlation with the
963 enzymatic hydrolysis of polysaccharides. Biotechnology for Biofuels. 2011;4(1):7.
964 77. Meng X, Ragauskas AJ. Recent advances in understanding the role of cellulose
965 accessibility in enzymatic hydrolysis of lignocellulosic substrates. Current Opinion in
966 Biotechnology. 2014;27:150-8.
967 78. Simmons TJ, Mortimer JC, Bernardinelli OD, Pöppler A-C, Brown SP, deAzevedo ER,
968 et al. Folding of xylan onto cellulose fibrils in plant cell walls revealed by solid-state NMR.
969 Nature Communications. 2016;7(1):13902.
970 79. Sheng Y, Lam SS, Wu Y, Ge S, Wu J, Cai L, et al. Enzymatic conversion of pretreated
971 lignocellulosic biomass: A review on influence of structural changes of lignin. Bioresource
972 technology. 2021;324:124631.

80. Ladeira Azar R, Sidnei E, Bordignon J, Laufer C, Specht J, Ferrier D, et al. Effect of Lignin Content on Cellulolytic Saccharification of Liquid Hot Water Pretreated Sugarcane Bagasse. Molecules. 2020;25:623.

81. Shimizu FL, de Azevedo GO, Coelho LF, Pagnocca FC, Brienzo M. Minimum Lignin and Xylan Removal to Improve Cellulose Accessibility. BioEnergy Research. 2020;13(3):775-85.

82. Zhang Y, Culhaoglu T, Pollet B, Melin C, Denoue D, Barrière Y, et al. Impact of Lignin Structure and Cell Wall Reticulation on Maize Cell Wall Degradability. Journal of agricultural and food chemistry. 2011;59(18):10129-35.

83. Yoo CG, Dumitrache A, Muchero W, Natzke J, Akinosho H, Li M, et al. Significance of Lignin S/G Ratio in Biomass Recalcitrance of Populus trichocarpa Variants for Bioethanol Production. ACS Sustainable Chemistry & Engineering. 2018;6(2):2162-8.

84. Besombes S, Mazeau K. The cellulose/lignin assembly assessed by molecular modeling. Part 2: seeking for evidence of organization of lignin molecules at the interface with cellulose. Plant Physiology and Biochemistry. 2005;43(3):277-86.

85. Araya F, Troncoso E, Mendonça R, Freer J. Condensed lignin structures and re-localization achieved at high severities in autohydrolysis of Eucalyptus globulus wood and their relationship with cellulose accessibility: Autohydrolysis of Eucalyptus globulus Wood. Biotechnology and Bioengineering. 2015;112.

86. Kumar R, Wyman CE. Cellulase adsorption and relationship to features of corn stover solids produced by leading pretreatments. Biotechnol Bioeng. 2009;103(2):252-67.

87. Xu H, Che X, Ding Y, Kong Y, Li B, Tian W. Effect of crystallinity on pretreatment and enzymatic hydrolysis of lignocellulosic biomass based on multivariate analysis. Bioresource technology. 2019;279:271-80.

997 88. Liao JJ, Latif NHA, Trache D, Brosse N, Hussin MH. Current advancement on the
998 isolation, characterization and application of lignin. International Journal of Biological
999 Macromolecules. 2020.
1000 89. El Hage F, Legland D, Borrega N, Jacquemot MP, Griveau Y, Coursol S, et al. Tissue
1001 Lignification, Cell Wall p-Coumaroylation and Degradability of Maize Stems Depend on
1002 Water Status. Journal of agricultural and food chemistry. 2018;66(19):4800-8.
1003 90. Méchin V, Argillier O, Rocher F, Hébert Y, Mila I, Pollet B, et al. In Search of a Maize
1004 Ideotype for Cell Wall Enzymatic Degradability Using Histological and Biochemical Lignin
1005 Characterization. Journal of agricultural and food chemistry. 2005;53(15):5872-81.
1006 91. Li Z, Yu Y, Sun J, Li D, Huang Y, Feng Y. Effect of Extractives on Digestibility of
1007 Cellulose in Corn Stover with Liquid Hot Water Pretreatment. BioResources. 2015;11(1).
1008 92. Overend RP, Chornet E, Gascoigne JA, Hartley BS, Broda PMA, Senior PJ.
1009 Fractionation of lignocellulosics by steam-aqueous pretreatments. Philosophical Transactions
1010 of the Royal Society of London Series A, Mathematical and Physical Sciences.
1011 1987;321(1561):523-36.
1012 93. Belmokhtar N, Habrant A, Lopes Ferreira N, Chabbert B. Changes in Phenolics
1013 Distribution After Chemical Pretreatment and Enzymatic Conversion of Miscanthus ×
1014 giganteus Internode. BioEnergy Research. 2013;6(2):506-18.
1015 94. Ho-Yue-Kuang S, Alvarado C, Antelme S, Bouchet B, Cézard L, Le Bris P, et al.
1016 Mutation in Brachypodium caffeic acid O-methyltransferase 6 alters stem and grain lignins and
1017 improves straw saccharification without deteriorating grain quality. Journal of experimental
1018 botany. 2016;67(1):227-37.
1019 95. Monties B. Dosage de la lignine insoluble en milieu acide: influence du prétraitement
1020 par hydrolyse acide sur la lignine Klason de bois et de paille. Agronomie. 1984;4:387-92.

96. Lapierre C, Monties B, Rolando C. Thioacidolysis of Poplar Lignins: Identification of Monomeric Syringyl Products and Characterization of Guaiacyl-Syringyl Lignin Fractions. Holzforschung. 1986;40(2):113.

97. Chandra R, Saddler J. Use of the Simons' Staining Technique to Assess Cellulose Accessibility in Pretreated Substrates. Industrial Biotechnology. 2012;8:230-7.

98. Kwok TT, Fogg DN, Realff MJ, Bommarius AS. Applying Direct Yellow 11 to a modified Simons' staining assay. Cellulose. 2017;24(6):2367-73.

99. Larsson PT, Wickholm K, Iversen T. A CP/MAS13C NMR investigation of molecular ordering in celluloses. Carbohydrate Research. 1997;302(1):19-25.

100. Newman RH. Estimation of the lateral dimensions of cellulose crystallites using 13C NMR signal strengths. Solid State Nuclear Magnetic Resonance. 1999;15(1):21-9.

101. Kolodziejski W, Klinowski J. Kinetics of Cross-Polarization in Solid-State NMR: A Guide for Chemists. Chem Rev. 2002;102(3):613-28.

102. Saunders M, Kim B, Maes C, Akle S, Zahr M. Primal-Dual Interior Method for Convex Objectives. 2012.

103. Adney B, Baker J, National Renewable Energy L. Measurement of cellulase activities : laboratory analytical procedure (LAP) : issue date, 08/12/1996 Golden, Colo.: National Renewable Energy Laboratory; 2008. Available from: http://purl.access.gpo.gov/GPO/LPS94126.

Figure legends:

Fig. 1: Kinetics of released monosaccharides yield during saccharification of raw and HWP samples. A) M7 samples, B) M9 samples.

Fig. 2: FTIR spectra of raw and pretreated (a) M7 and (b) M9 samples.

Fig. 3: Schematic representation of raw cellulose fibril and cell wall organization. a) Schematic representation of raw cellulose fibril with the representation of the four cellulose forms and the two fibril aggregate dimensions: lateral fibril dimension (LFD), and lateral fibril aggregate dimensions (LFAD) (Adapted from **(56)**); Schematic representation of cellulose microfibrils distribution within lignocellulosic matrix and of the T1ρH and THH variations of b) raw sample and c) HWP sample according to the hemicellulose loss and lignin condensation.

Fig. 4: Evolution of the total adsorbed dye and DY11/DB1 ratio of raw and pretreated samples. The total adsorbed dye are represented by bars with left axis and DY11/DB1 ratio by plots with the right axis. The M7 values are represented in white and M9 samples in gray.

Fig. 5: T_2 distribution for (a) M7 and (b) M9 samples with a water content of 20 % (w/w). The x axis is the logarithmic scale of the relaxation time. The Y axis corresponds to the distribution amplitude expressed in normalized relative water content (% w/w). The replicates are represented in the same color.

Fig. 6: T_2 distribution for (a) M7 and (b) M9 samples with a water content of 80% (w/w). The x axis is the logarithmic scale of the relaxation time. The Y axis corresponds to the distribution amplitude expressed in normalized relative water content (% w/w). The correspondence between the relaxation time (T_2) and the meso-porosity is indicated at the top of the figure. The experiments were realized in duplicate. The grey area, between 5 and 15 nm, corresponds to the range of pore size available for enzymes, the replicates are represented in the same color.

Fig. 7: Pearson's correlation coefficients between physico-chemical factors variations and hydrolysis yield after 72h. The red squares correspond to negative correlations and the blue squares to positive correlations. Values in bold are significant with a p-values ≤ 0.05 and * have a p-values ≤ 0.01.

Additional files:

Additional file 1 TIF: Pearson's correlation matrix calculated between two variables. The red squares correspond to negative correlations and the blue squares to positive correlations. Values in bold are significant (p-values ≤ 0.05).

Additional file 2 XLS: Relaxation time (T_2) values, water proportion (P_2) and pick width proportion (PW%) of the peaks represented in the figure 5. The PW was normalized to the T_2 value. Results are expressed as means of 3 repetitions with standard deviation into parenthesis.

Additional file 3 XLS: Relaxation time (T_2) values, water proportion (P_2) and pick width proportion (PW%) of the peaks represented in the figure 6. The PW was normalized to the T_2 value. Results are expressed as means of 3 repetitions with standard deviation into parenthesis.

Figures

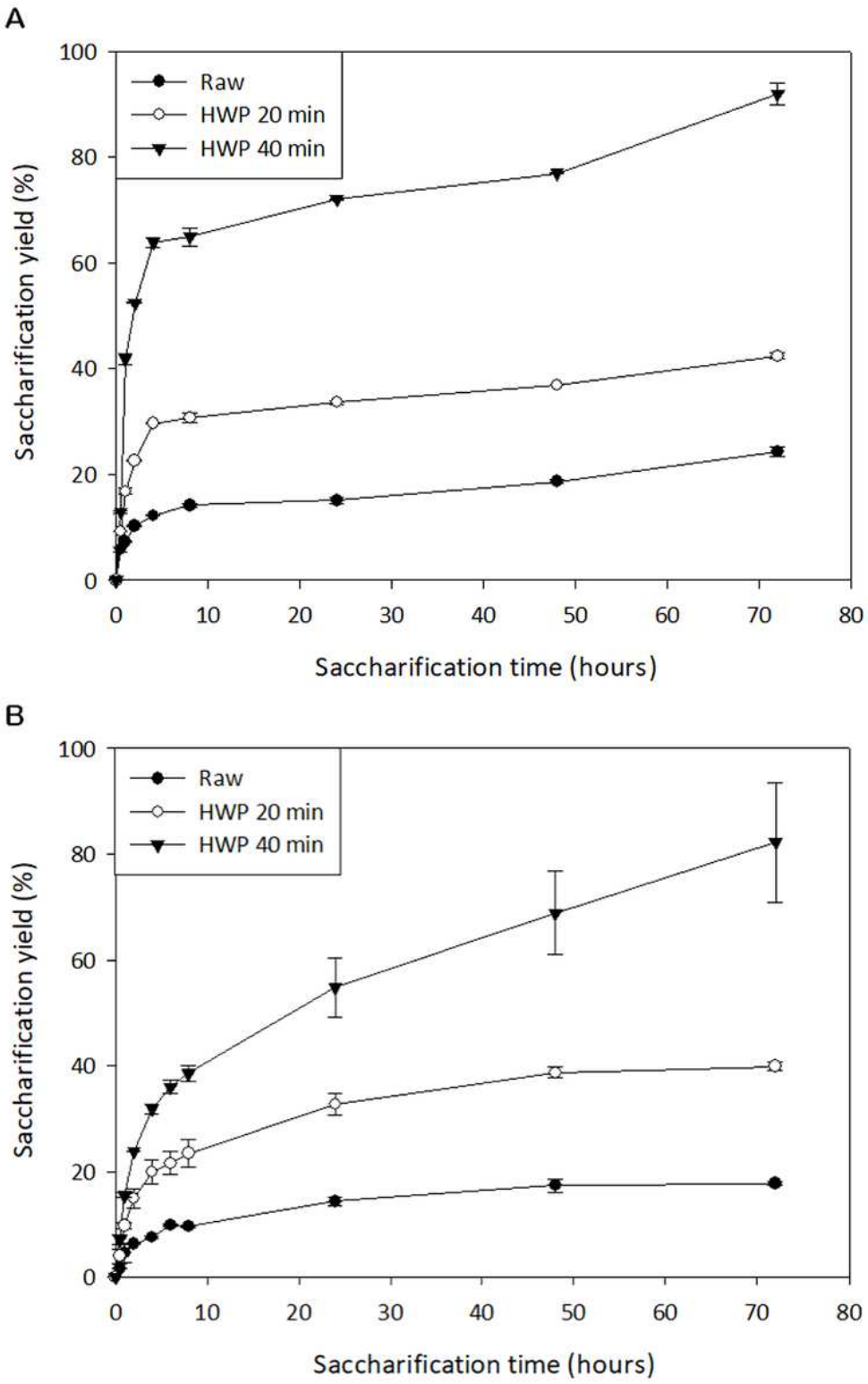

Figure 1

Kinetics of released monosaccharides yield during saccharification of raw and HWP samples.

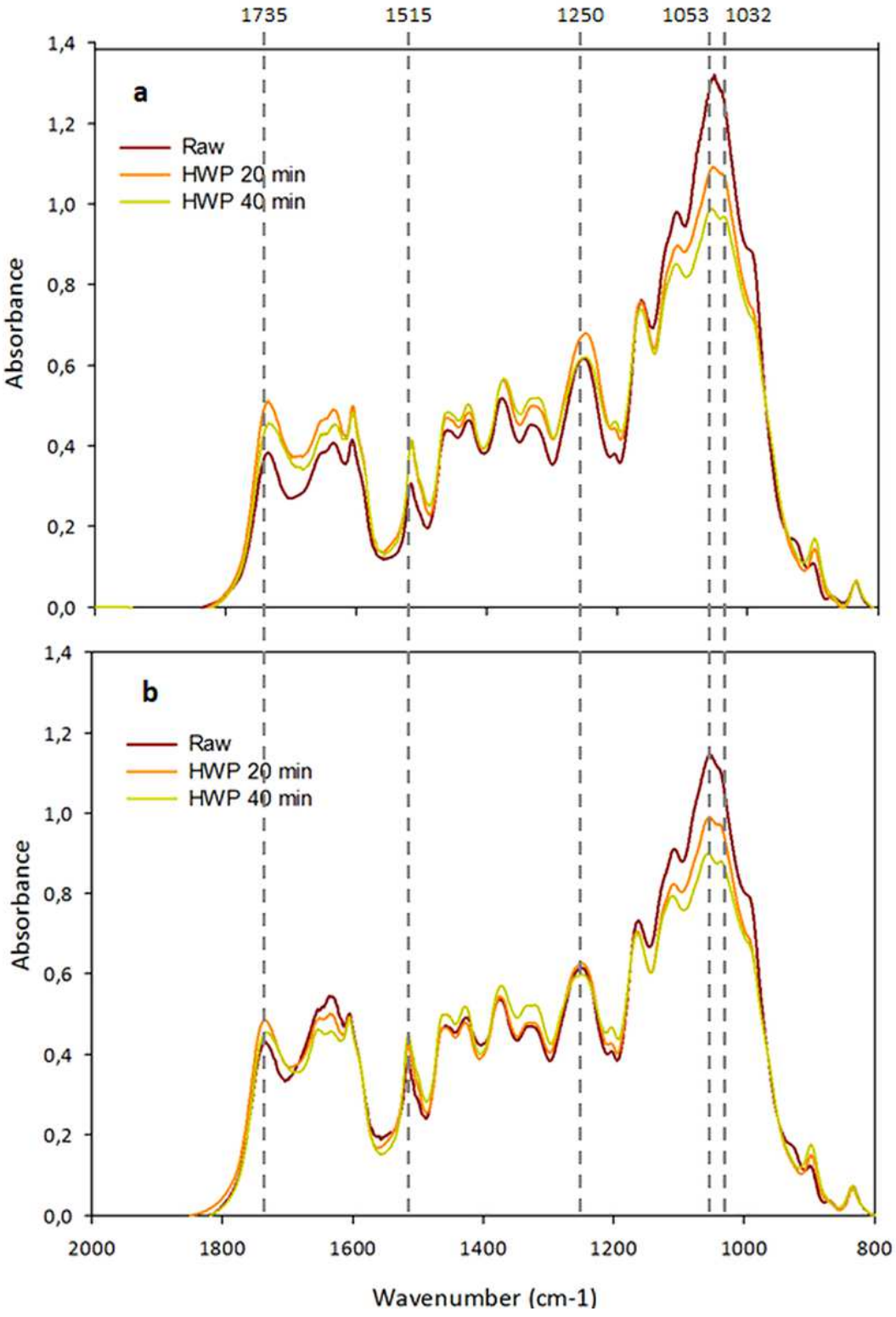

Figure 2

FTIR spectra of raw and pretreated (a) M7 and (b) M9 samples.

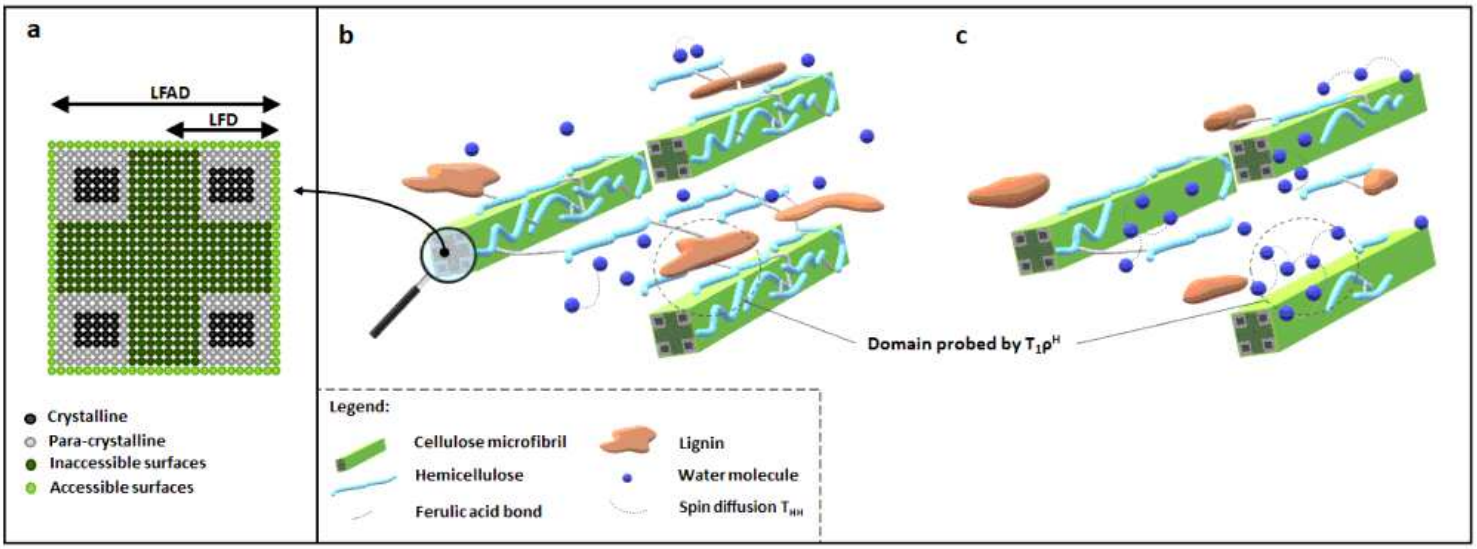

Figure 3

Schematic representation of raw cellulose fibril and cell wall organization.

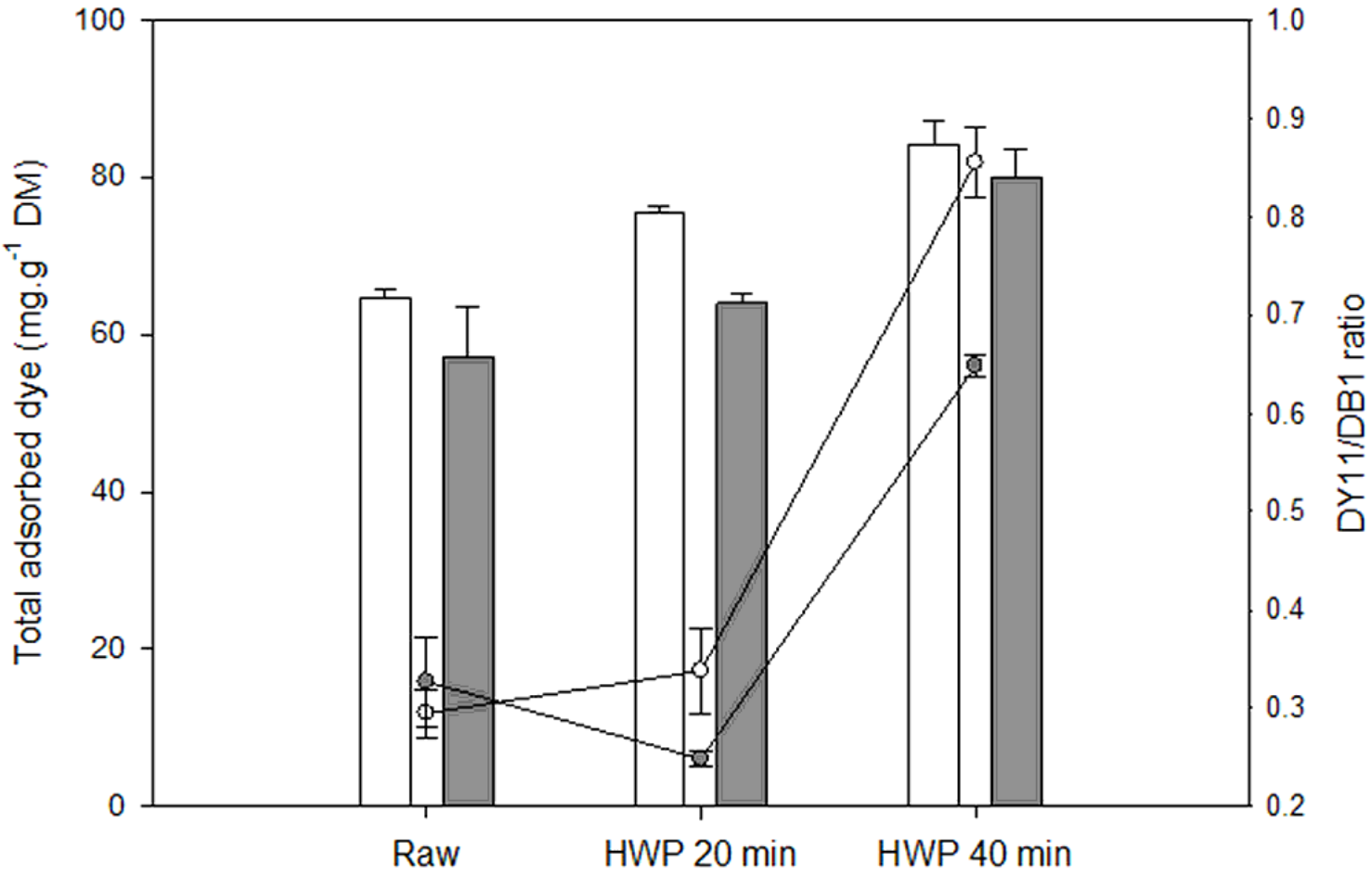

Figure 4

Evolution of the total adsorbed dye and DY11/DB1 ratio of raw and pretreated samples.

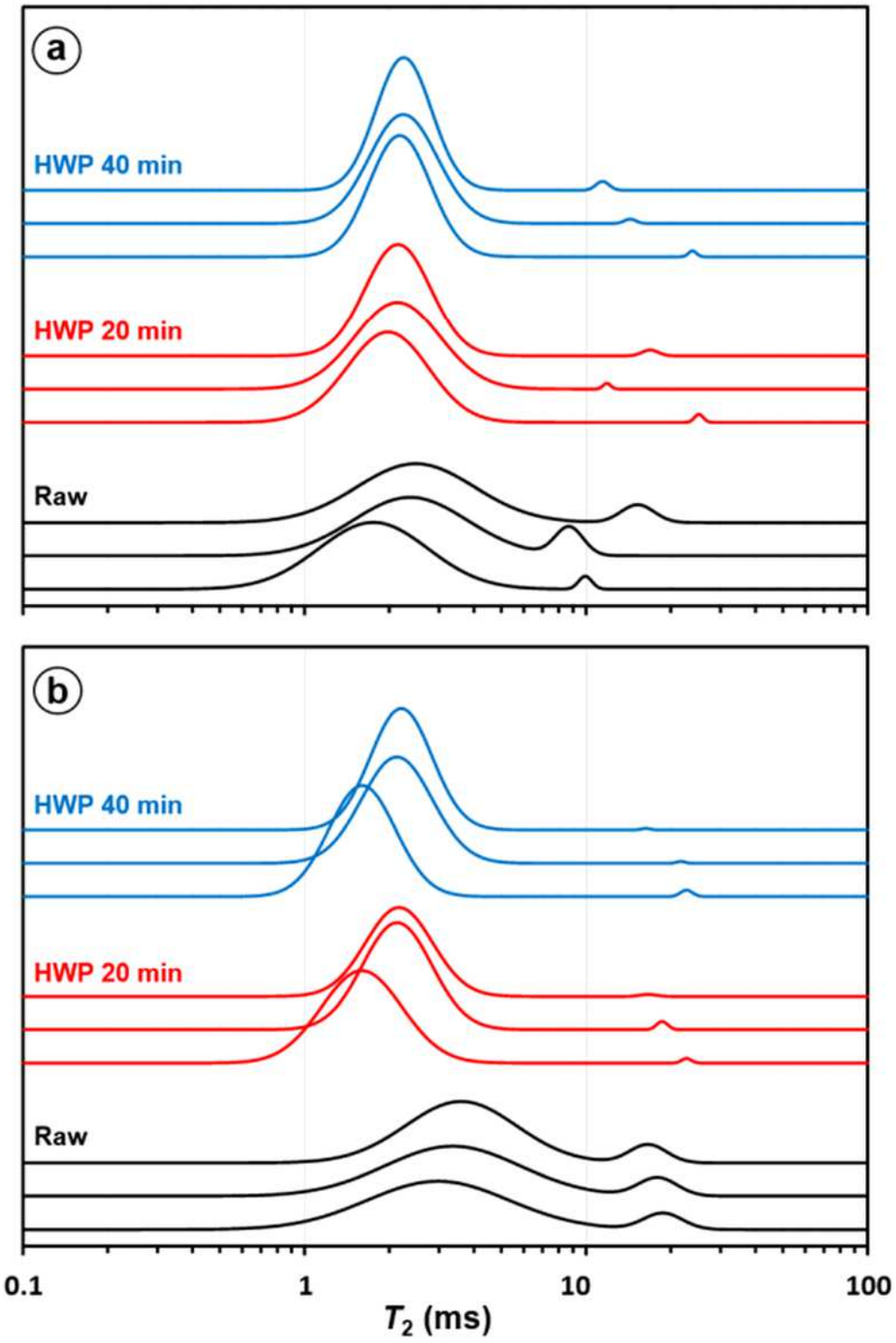

Figure 5

T2 distribution for (a) M7 and (b) M9 samples with a water content of 20 % (w/w).

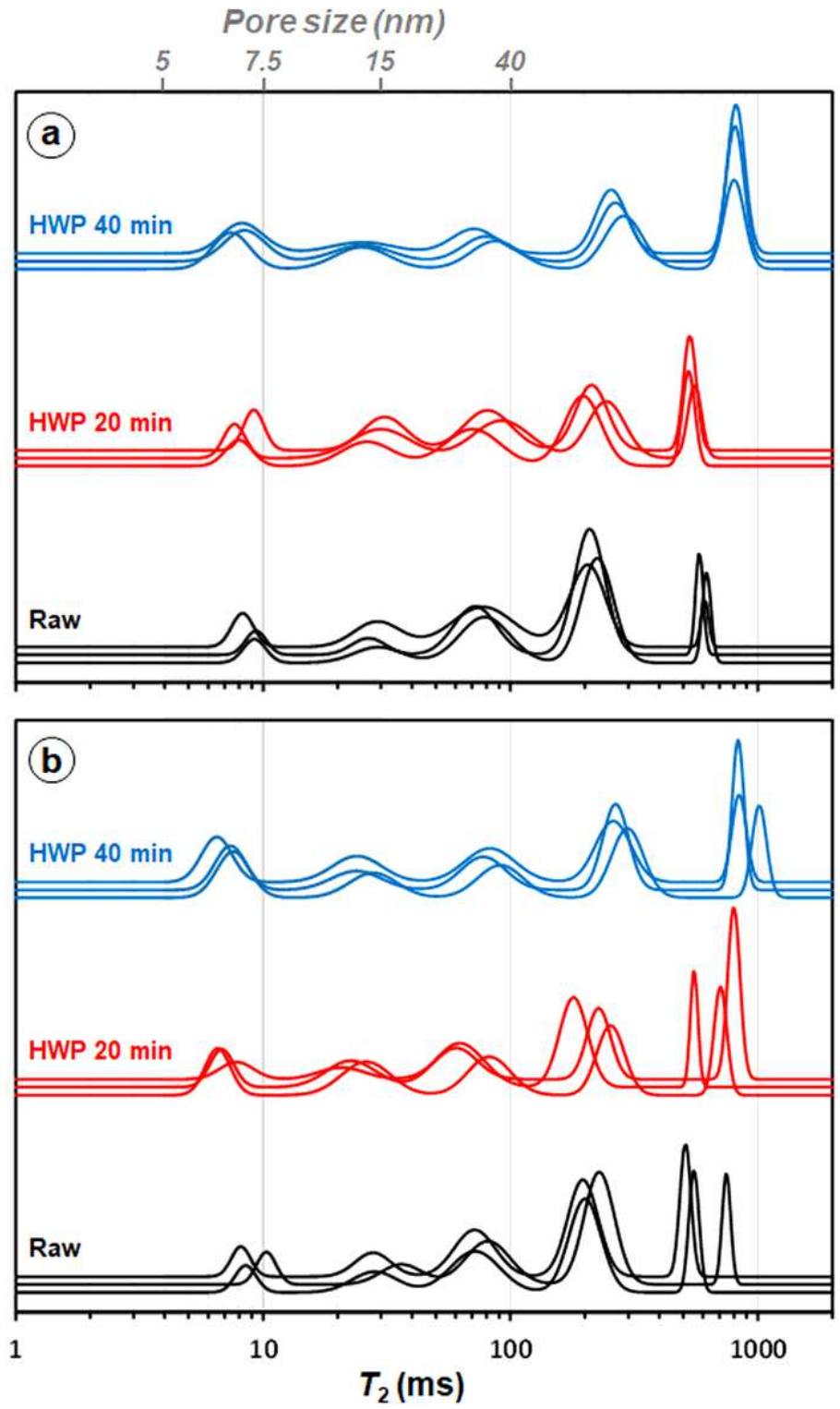

Figure 6

T2 distribution for (a) M7 and (b) M9 samples with a water content of 80% (w/w).

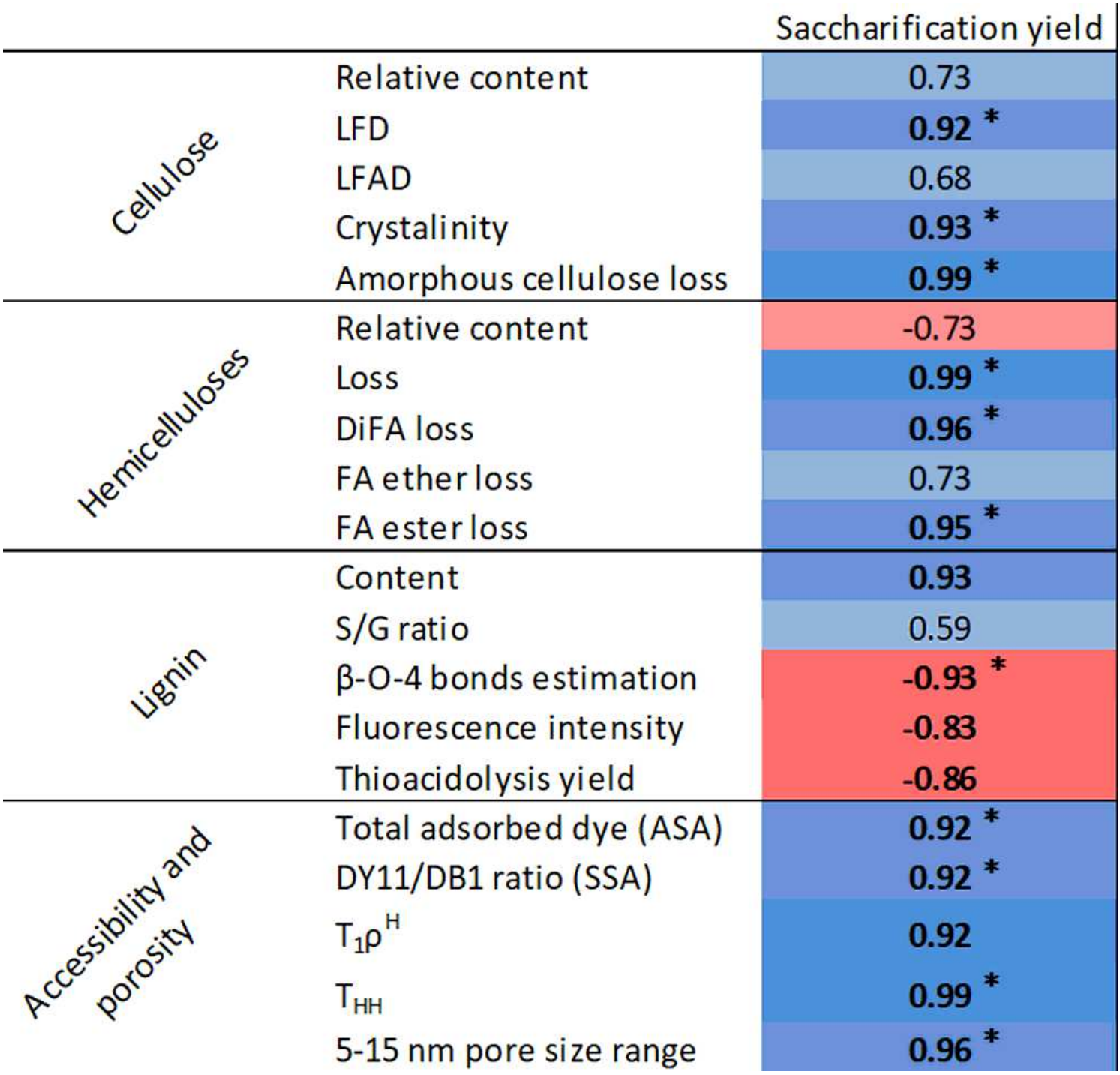

Figure 7

Pearson's correlation coefficients between physico-chemical factors variations and hydrolysis yield after 72h.

Supplementary Files

This is a list of supplementary files associated with this preprint. Click to download.

- Additionalfile1.tif

- Additionalfile2.xlsx
- Additionalfile3.xlsx